AFRL-OSR-VA-TR-2014-0197

ULTRAFAST PHOTORESPONSIVE STARBURST AND DENDRITIC FULLERENYL NOSTRUCTURES FOR BROADBAND NONLINEAR PHOTONIC MATERIAL APPLICATIONS

Long Chiang
MASSACHUSETTS UNIVERSITY OF LOWELL MA

08/20/2014
Final Report

Air Force Research Laboratory
AF Office Of Scientific Research (AFOSR)/ RTD
Arlington, Virginia 22203
Air Force Materiel Command

REPORT DOCUMENTATION PAGE

Form Approved
OMB No. 0704-0188

PLEASE DO NOT RETURN YOUR FORM TO THE ABOVE ADDRESS.

1. REPORT DATE *(DD-MM-YYYY)*	2. REPORT TYPE	3. DATES COVERED *(From - To)*
05-08-2014	Final Report	03-01-2009 – 05-31-2014

4. TITLE AND SUBTITLE

Ultrafast Photoresponsive Starburst and Dendritic Fullerenyl Nanostructures for Broadband Nonlinear Photonic Material Applications

5a. CONTRACT NUMBER

5b. GRANT NUMBER
FA9550-09-1-0183

5c. PROGRAM ELEMENT NUMBER

6. AUTHOR(S)

Long Chiang

5d. PROJECT NUMBER

5e. TASK NUMBER

5f. WORK UNIT NUMBER

7. PERFORMING ORGANIZATION NAME(S) AND ADDRESS(ES)

Department of Chemistry, University of Massachusetts Lowell, 1 University Avenue, Lowell, MA 01854

8. PERFORMING ORGANIZATION REPORT NUMBER

9. SPONSORING/MONITORING AGENCY NAME(S) AND ADDRESS(ES)

Dr. Charles Lee, AFOSR/RSA, 875 North Randolph Street, Suite 325, Arlington, VA 22203-1954

10. SPONSOR/MONITOR'S ACRONYM(S)

11. SPONSORING/MONITORING AGENCY REPORT NUMBER

12. DISTRIBUTION AVAILABILITY STATEMENT
Approved for Public Release

13. SUPPLEMENTARY NOTES

14. ABSTRACT

We demonstrated the design, synthesis, structural characterization, and study of photophysical properties of ultrafast photoresponsive starburst and dendritic C_{60}/C_{70}-light harvesting antenna-based organic nanostructures for broadband nonlinear optical (NLO) nanomaterial applications. These organic NLO nanostructures exhibit both ultrafast photoresponse and a large cross-section of two-photon absorption (2PA) throughout a wide NIR spectrum may make them also suitable for use as nonlinear biophotonic materials. With hybrid C_{60}-(antenna)$_x$ analogous as branched triad and tetrad starburst nanostructures, 2PA characteristics at multiple NIR wavelengths provided support for their suitability in uses as broadband NLO nanomaterials at 600–1100 nm that includes the 2PA ability of two antenna, DPAF (700–850 nm) and CPAF (850–1100 nm), and the fullerene cage at shorter wavelengths (600–700 nm) to build broadband NLO characteristics. A new molecular encapsulation of C_{70}-(antenna)$_{1or2}$ conjugates by helical *st*-PMMA was also perform.

15. SUBJECT TERMS

16. SECURITY CLASSIFICATION OF:			17. LIMITATION OF ABSTRACT	18. NUMBER OF PAGES	19a. NAME OF RESPONSIBLE PERSON
a. REPORT	b. ABSTRACT	c. THIS PAGE	No	26	Long Chiang
					19b. TELEPONE NUMBER (*Include area code*) (978)-934-3663

TABLE OF CONTENTS

Section **Page**

1.0 SUMMARY

The project is aimed to design, synthesis, structural characterization, and study of photophysical properties of ultrafast photoresponsive starburst and dendritic C_{60}/C_{70}-light harvesting antenna-based organic nanostructures for broadband nonlinear optical (NLO) nanomaterial applications. The main focus of research is to investigate the controllability of molecular geometrical 3D-configuration of 2PA-based multibranched NLO chromophore materials to (i) enhance 2PA cross-sections (σ_2) and optical limiting (OL) efficiency, (ii) limit the size of cluster formation (certain small cluster sizes with twisted conformers may increase σ_2 while a larger size with chromophore-stacking decreases it), (iii) increase geometrical steric hindrance in 3D configuration to provide 3D-molecular separation/spacing while forming small clusters, and (iv) minimize the excimer formation, self-quenching process, and triplet–triplet annihilation while forming an organized self-assembly structures (fullerosome, tubular, etc.),

We synthetically construct starburst C_{60}/C_{70}-(antenna)$_x$ (x = 1–4, where antenna are DAPF-C_n and CPAF-C_n) and modify the fused, multibranched [C_{60}-antenna]$_3$ nanostructures as a 3D tris-analogous with three C_{60}-DPAF-C_n units sharing one common benzene that resulted in an unexpected major product of *cis*-cup conformer, with three fluorescent DPAF-C_n rings facing each other at the top-sides of the cup. This 3-D geometrical configuration of the nanostructure eliminates potential direct $\pi-\pi$ stacking interactions of either $C_{60}-C_{60}$ or DPAF−DPAF moieties that was proposed to reduce the concern of (iv) during molecular self-assemblies and materials engineering processing and increase 2PA cross-section values. In the other specific new approach, we have developed a new helical *syndiotactic*-PMMA wrapping methods to perform molecular encapsulation of C_{70}-(antenna)$_{1or2}$ conjugates to a form of peapod-like two-photon absorbers inside the *s*-PMMA polymer helix. The molecular wrapping was intended to eliminate any concern of (iv) and align 2PA nanostructures to the linear configuration of a peapod chain with a large length-vs-width spatial ratio that may allow the study of this physical relationship to two-photon absorption cross-sections and the high film transparency/visibility.

We also demonstrated C_{60}-(antenna)$_x$ analogous nanostructures having branched hybrid triad C_{60}(>DPAF-C_{18})(>CPAF-C_{2M}) and tetrad C_{60}(>DPAF-C_{18})(>CPAF-C_{2M})$_2$. The structural design was intended to facilitate the ultrafast fs intramolecular energy-transfer from photoexcited C_{60}[>^{1}(DPAF)*-C_{18}](>CPAF-C_{2M})$_{1or2}$ or C_{60}(>DPAF-C_{18})[>^{1}(CPAF)*-C_{2M}]$_{1or2}$ to the C_{60}> cage moiety upon two-photon pumping at either 780 or 980 nm, respectively. The latter nanostructure showed approximately equal extinction coefficients of optical absorption over 400–550 nm that corresponds to near-IR two-photon based excitation wavelengths at 780–1100 nm for broadband nonlinear optical (NLO) applications. Aside from their enhanced two-photon absorption (2PA) activity at 780 nm, we also demonstrated ultrafast photo-responses at 980 nm showing 2PA cross-section (σ_2) values of 995–1100 GM for the hybrid tetrad. These σ_2 values were correlated to the observed good efficiency in reducing fs light-transmittance down to 35% at the light intensity of 110 GW/cm^2. Accordingly, 2PA characteristics of these nanostructures at multiple NIR wavelengths provided support for their suitability in uses as broadband NLO nanomaterials at 600–1100 nm that includes the 2PA ability of two antenna, DPAF (700–850 nm) and CPAF (850–1100 nm), and the fullerene cage at shorter wavelengths (600–700 nm) to build broadband NLO characteistics.

We found that the molecular wrapping of linear regiospecific dipolar C_{70}(>DPAF-C_2)$_2$ and C_{70}(>DPAF-C_{2M})$_2$, and the hybrid bisadduct C_{70}(>DPAF-C_2)(>CPAF-C_{2M}) (one DPAF antenna located at a cage pole and the other antenna located at the opposite cage pole area) by helical *st*-PMMA led to observation of broadband characteristics at 780 and 980 nm with 2PA cross-section values of ~1227 GM (125 fs, 780 nm, toluene), higher than that (940 GM) without wrapping and much higher than C_{60} analogous (220 GM). Most importantly, all C_{70}(>DPAF-C_2)$_2$@*st*-PMMA, C_{70}(>DPAF-C_{2M})$_2$@*st*-PMMA, C_{70}(>DPAF-C_2)(>CPAF-C_{2M})@*st*-PMMA showed transmittance reductions down to <5% at 200–300 GW/cm^2 in toluene (5.0×10^{-3} M), the lowest % value among our C_{60}/C_{70}-(antenna)$_x$ found to date. The same encapsulated nanomaterials were casted as a thin film (0.1 mm thickness) to show

excellent transparency with light-transmittance of C_{70}(>DPAF-C_2)$_2$@*st*-PMMA (125 fs, 780 nm) measured at <22% at 300 GW/cm^2.

2.0 INTRODUCTION

The development of broadband nonlinear optical (NLO) organic nanostructures is an ever expanding area of research. This field requires the design of sophisticated, processable functional NLO materials for (i) surface coating[1–3] and (ii) two-photon absorption (2PA) based photodynamic therapy[4–8] (2γ-PDT) against pathogens and cancer to minimize the damage to surrounding normal tissue. Photoresponsive complex fullerene derivatives[9–16] and a number of organic chromophores[17–20] have been found to exhibit enhanced nonlinear photonic behavior under intense light radiation.[21,22] These NLO characteristics[23] have been induced by both simultaneous multiphoton absorption (MPA) and excited singlet state-based reverse saturable absorption (RSA)[24,25] in the fs to ps region, excited triplet state absorption in ns, and induced nonlinear thermal scattering (NLS) in the sub-ns to ns region.

Nonlinear optical absorption features of fullerenes and their derivatives is based on excited-state RSA events in the long-visible–NIR region and effective 2PA processes in the NIR region.[26] C_{60} is more readily available in up to kilogram quantities than higher fullerenes. However, its visible absorption extinction coefficient is low. Therefore, many highly visible-light absorptive chromophores, such as porphyrins and phthalocyanines, were commonly applied to induce excited-state electron-transfer or fluorescence energy-transfer events for enhancing photophysical properties of fullerenes or their derivatives.[27–30] We circumvented this encumbrance by attaching highly fluorescent chromophores as light-harvesting antenna units, such as dialkyldiphenylaminofluorene (DPAF-C_n), to enhance visible absorption and 2PA cross-sections in the NIR,[11,14,15] Specifically, covalent attachment of this type of antenna donor chromophore to a C_{60} molecule (electron-acceptor) was accomplished via periconjugation with a physical separation distance of only <3.5 Å between donor and acceptor moieties. This led to the realization of ultrafast intramolecular energy- and/or electron-transfer from photoexcited antenna moiety to C_{60} in <130–150 fs[15] that made the corresponding C_{60}-antenna conjugates, C_{60}(>DPAF-C_n)$_x$, capable of exhibiting photoresponse in a nearly instantaneous time scale to protect against high-intensity radiation. By increasing the number of attached antennae to four per C_{60} cage giving starburst pentad nanostructures, highly enhanced fs 2PA cross-section values were observed in a concentration-dependent manner.[31]

Meanwhile, alteration of the electron-withdrawing ability of the covalent bridging unit between C_{60} and the antenna from a keto group to a 1,1-dicyanoethylenyl (DCE) group led to large bathochromic shift of the linear optical absorption of the resulting chromophore, for example C_{60}(>CPAF-C_2) moves from 410 nm (λ_{max}) to 503 nm with the shoulder band extended beyond 550 nm in the UV-vis spectrum. The shift considerably increased its light-harvesting ability in visible wavelengths and led to a nearly 6-fold higher in the production quantum yield of singlet oxygen ($^1O_2$) from C_{60}(>CPAF-C_{2M}) as compared with that of C_{60}(>DPAF-C_{2M}). The mechanism of $^1O_2$ production was due to the intermolecular triplet-energy transfer from the ^{3}(C_{60}>)* cage moiety to $^3O_2$. A large increase in the production of reactive oxygen species (ROS) by excited C_{60}(>CPAF-C_{2M}) explained its effective photokilling of HeLa cells *in vitro*, via 1γ-PDT.[32] The observation demonstrated the intramolecular/intramolecular interaction between the excited CPAF-C_n donor antenna moiety and the acceptor C_{60} cage that was also confirmed by transient absorption spectroscopic measurements using ns laser pulses at 480–500 nm.[33] The behavior resembles that of DPAF-C_n antenna with transient photoexcitation at 380–410 nm reported previously.[34] By extending the same intramolecular photophysical properties to 2PA-based excitation applications, these C_{60}-(antenna)$_x$ analogous nanostructures may be utilized as potential photosensitizers for 2γ-PDT at either 800 nm (with DPAF antenna) or 1000 nm (with CPAF antenna) that is well-suited to the biological optical window of 800–1100 nm. Accordingly, selective attachment of combined DPAF-C_n and CPAF-C_n antenna moieties as hybrid chromophore addends to a single C_{60} cage should result in the

formation of fullerenyl multiadducts capable of facilitating both dual-band 2γ-PDT ability and broadband NLO by high-power radiation.[35]

Fullerenes are nanocarbon cages with all sp^2 carbons interlinked in a structure of hollow sphere. Highly strained curving regions of the cage surface consist of chemically reactive six fulvalenyl bridging olefins that can be utilized for making nucleophilic addition reactions. Chemical modification of C_{60} on only a limit number of functionalization sites may not lead to much alternation of the cage's photophysical properties. Conversely, nucleophilic addition of one or two light-harvesting antenna chromophores will largely enhance the cage's ability to respond and perform various photoinduced electronic and energy-related events by acting as an electron-acceptor.[36,37] The most abundant [60]fullerene is more readily available commercially in up to kilogram quantities than a number of higher fullerenes. However, its visible absorption extinction coefficient is rather low. This limitation can be overcome by attaching highly fluorescent chromophores as light-harvesting antenna units, such as porphyrin[38,39] or dialkyldiphenylaminofluorene (DPAF-C_n), to enhance visible absorption of the resulting conjugates and, in the latter cases, 2PA cross-sections in the NIR wavelengths.[11, 14,15] The absorbed photoenergy by the donor antenna was able to undergo efficient intramolecular transfer to the fullerene acceptor moiety, leading to the generation of $^1(C_{60}>)^*$. Triplet energy transfer from $^3(C_{60}>)^*$ to molecular oxygen produces singlet oxygen ($^1O_2$) excited triplet cage state $^3(C_{60}>)^*$ after the intersystem crossing from its excited singlet state that gives the cytotoxic effect to the cells in the Type-II photochemistry.[40,41]

3.0 METHODS, ASSUMPTIONS, AND PROCEDURES

3.1 Materials

Reagents of 1,8-diazabicyclo[5,4,0]-undec-7-ene (DBU), 1-bromooctadecane, 2-bromofluorene, sodium *t*-butoxide, potassium *t*-butoxide, aluminum chloride, titanium chloride, *rac*-BINAP, *tris*(dibenzylideneacetone)dipalladium(0), malononitrile, and 2-methoxy-ethanol, were purchased from Aldrich Chemicals and used without further purification. The chemical 1-bromooctadecane was purchased from Tokyo Chemical Industry Co., Ltd. A C_{60} sample with a purity of 99.0% was purchased from Term USA, Inc. Both $C_{60}(>DPAF\text{-}C_{18})_2$ and $C_{60}(>CPAF\text{-}C_{2M})_2$ were synthesized by the similar methods described below.

3.2 Synthetic Procedures

*Synthesis of 9,9-di(2-methoxyethyl)-2-diphenylaminofluorene, DPAF-C_{2M} (**6**).* Part A: In a round-bottom flask containing a mixture of triethylamine (19.9 mL, 0.14 mol), 2-methoxyethanol (10.3 mL, 0.13 mol), and anhydrous dichloroethane (150 mL) at 0 ^oC was added methane sulfonyl chloride (11.1 mL, 0.14 mol) over a period of 20 min. The mixture was warmed to ambient temperature under a nitrogen atmospheric pressure and stirred for 12 h. It was quenched by the addition of water and washed with water (2 × 150 mL), dilute hydrochloric acid (1 × 100 mL), and saturated sodium bicarbonate (1 × 100 mL) in sequence. The organic layer was dried over sodium sulfate and concentrated *in vacuo*. The crude brownish liquid was vacuum distilled at 120−130 °C to afford 2-methoxyethylmethanesulfonate (17.9 g) in a nearly quantitative yield; ^1H NMR (500 MHz, $CDCl_3$, ppm) δ 4.36 (t, J = 4.41 Hz, 2H), 3.66 (t, J = 4.41 Hz, 2H), 3.40 (s, 3H), and 3.05 (s, 3H).

Part B: In a round-bottom flask containing a mixture of 2-diphenylaminofluorene **5** (DPAF) (0.52 g, 1.56 mmol) and potassium *t*-butoxide (0.38 g, 3.39 mmol) in dry THF (30 mL) at 0 ^oC was added 2-methoxyethylmethanesulfonate (10.53 g, 3.4 mmol) over 10 min. The mixture was warmed to ambient temperature under a nitrogen atmosphere and stirred for 4.0 h. The reaction mixture was washed with brine (20 mL) and water (20 mL). Organic layer was dried over sodium sulfate and concentrated *in vacuo*. The crude product was then purified by column chromatography [silica gel, toluene−ethyl acetate (3:1) as the eluent] via a chromatographic fraction corresponding to R_f = 0.7 on TLC (SiO_2) with the same eluent to afford DPAF-C_{2M} **6** as white solids in a yield of 94% (0.66 g). Spectroscopic data:

MALDI-MS (TOF) *m/z* 449 calculated for $^{12}C_{31}{}^{1}H_{31}{}^{14}N_{1}{}^{16}O_{2}$; found, *m/z* 450 ($MH^+$); ^{1}H NMR (500 MHz, $CDCl_3$, ppm) δ 7.61 (d, J = 7.60 Hz, 1H), 7.55 (d, J = 7.55 Hz, 1H), 7.38 (d, J = 7.37 Hz, 1H), 7.31 (t, J = 7.32 Hz, 1H), 7.28−7.24 (m, 5H), 7.18−7.10 (m, 6H),), 7.13−7.00 (m, 2H), 3.04 (s, 6H), 2.79−2.71 (m, 4H), and 2.26−2.20 (m, 4H); ^{13}C NMR (125.77 MHz, $CDCl_3$, ppm) δ 150.66, 149.32, 148.32, 147.95, 140.67, 135.72, 129.67, 127.79, 127.08, 124.43, 124.12, 123.18, 120.98, 119.69, 69.08, 58.77, 51.45, and 39.76.

*Synthesis of 7-α-bromoacetyl-9,9-di(2-methoxyethyl)-2-diphenylaminofluorene, BrDPAF-C_{2M} (**7**).* To a suspension of aluminum chloride (4.8 g, 36 mmol) in 1,2-dichloroethane (200 mL) at 0 ^{o}C was added a solution of DPAF-C_{2M} **6** (5.44 g, 12.1 mmol) in 1,2-dichloroethane (50 mL). It was added α-bromoacetyl bromide (2.44 g, 12.1 mmol) over a period of 10 min. The mixture was stirred for 4.0 h at 0 ^{o}C. The solution was worked up by slow addition of dilute HCl (1.0 N) solution (50 mL) while maintaining the temperature at 0 ^{o}C. The resulting organic layer was washed subsequently with dilute brine (2 × 50 mL) and water (2 × 50 mL) at room temperature and dried over magnesium sulfate. It was followed by the solvent removal *in vacuo*. The crude products were purified by column chromatography [silica gel, hexane−ethyl acetate (4:1) as the eluent] at its chromatographic band corresponding to R_f = 0.2 on TLC (SiO_2) with the same eluent to afford BrDPAF-C_{2M} **7** in 91 % yield (6.3 g). Spectroscopic data: FT-IR (KBr) ν_{max} 3054 (w), 3037 (w), 2925 (m), 2871 (m), 2804 (w), 1693(w), 1673 (m), 1593 (s), 1490 (s), 1467 (m), 1430 (w), 1388 (w), 1320 (w), 1279 (s), 1194 (w), 1113 (m), 1026 (w), 820 (w), 754 (m), 697 (m), 669 (w), and 627 (w) cm^{-1}; UV-vis ($CHCl_3$) λ_{max} (ε) 299 (1.4×10^4) and 407 (2.1×10^4 L/mol-cm); ^{1}H NMR (500 MHz, $CDCl_3$, ppm) δ 8.03−7.99 (m, 2H), 7.69 (d, J = 7.6 Hz, 1H), 7.63 (d, J = 7.5 Hz, 1H), 7.34−7.09 (m, 10H), 7.08−7.06 (m, 2H), 4.53 (s, 2H), 3.06 (s, 6H), 2.84−2.75 (m, 4H), and 2.33−2.21 (m, 4H); ^{13}C NMR (126 MHz, $CDCl_3$) δ 190.99, 151.81, 149.32, 149.20, 147.42, 146.14, 132.83, 131.74, 129.38, 129.29, 124.66, 123.46, 122.80, 121.81, 119.06, 117.86, , 68.52, 58.29, 51.30, 38.89, and 31.05.

*Synthesis of 7-α-bromoacetyl-9,9-dioctadecyl-2-diphenylaminofluorene, BrDPAF-C_{18} (**8**).* Part A: In a round-bottom flask containing a mixture of 2-diphenylaminofluorene 5 (DPAF, 1.0 g, 3.0 mmol), potassium *t*-butoxide (1.0 g, 8.9 mmol) in dry THF (30 mL) at 0 ^{o}C was added 1-bromooctadecane (2.0 g, 6.0 mmol) over 10 min. The mixture was warmed to ambient temperature under a nitrogen atmosphere and stirred overnight. The reaction mixture was washed with brine (40 mL) and water (40 mL) in sequence. The organic layer was dried over sodium sulfate and concentrated *in vacuo*. The crude product was purified by column chromatography [silica gel, hexane−toluene (4:1) as the eluent] as a chromatographic fraction corresponding to R_f = 0.8 on TLC (SiO_2) with the same eluent to give 9,9-dioctadecanyl-2-diphenylaminofluorene DPAF-C_{18} in 97% yield (2.44 g). Spectroscopic data: FT-IR (KBr) ν_{max} 3067 (w), 3036 (w), 2924 (s), 2853 (s), 1599 (m), 1494 (m), 1451 (w), 1331 (w), 1277 (m), 1154 (w), 1075 (w), 1029 (w), 824 (w), 751 (m), 737 (m), 696 (m), 623 (w), and 513 (w) cm^{-1}; MALDI-MS (TOF) *m/*z 838 calculated for $^{12}C_{61}{}^{1}H_{91}{}^{14}N_{1}$; found, *m/z* 839 ($MH^+$); ^{1}H NMR (500 MHz, $CDCl_3$, ppm) δ 7.63 (d, J = 6.9, 1H), 7.58 (d, J = 68.2, 1H), 7.33−7.25 (m, 7H), 7.15−7.13 (m, 5H), 7.05−7.01 (m, 3H), 1.93−1.81 (m, 4H), 1.33−1.07 (m, 60H), 0.91 (t, J = 6.94 Hz, 6H), and 0.73−0.62 (m, 4H); ^{13}C NMR (125 MHz, $CDCl_3$, ppm) δ 152.50, 148.45, 147.44, 141.29, 136.81, 129.52, 124.12, 123.98, 123.09, 122.78, 120.70, 119.93, and 119.49.

Part B: To a suspension of aluminum chloride (0.32 g, 2.4 mmol) in 1,2-dichloroethane (50 mL) at 0 ^{o}C was added a solution of DPAF-C_{18} (1.0 g, 1.2 mmol) in 1,2-dichloroethane (30 mL). It was then added by α-bromoacetyl bromide (0.30 g, 1.5 mmol) over 10 min. The mixture was stirred for 4.0 h at 0 ^{o}C. The solution was diluted by a slow addition of water (100 mL) while maintaining the reaction mixture temperature below 0 ^{o}C. The resulting organic layer was washed subsequently with dilute hydrochloric acid (1.0 N, 30 mL) and water (2 × 30 mL), and dried over magnesium sulfate followed by the solvent removal *in vacuo*. The crude yellow oil was purified by column chromatography [SiO_2, hexane−EtOAc (19:1) as the eluent] to afford BrDPAF-C_{18} **8** in 96 % yield (1.3 g). The product gave a chromatographic R_f at 0.5 on TLC (SiO_2) with the same eluent. Spectroscopic data: FT-IR (KBr) ν_{max} 3063 (w), 3034 (w), 2923 (s), 2852 (s), 1677 (m), 1595 (m), 1493 (m), 1466 (w), 1346 (w), 1279 (m),

1182 (w), 1027 (w), 819 (w), 753 (w), 697 (m), 620 (w), and 508 (w) cm^{-1}; UV-vis ($CHCl_3$) λ_{max} (ε) 292 (1.9×10^4) and 407 (2.5×10^4 L/mol-cm); ^{1}H NMR (500 MHz, $CDCl_3$, ppm) δ 7.95 (d, J = 8.18 Hz, 1H), 7.93 (s, 1H), 7.64 (d, J = 7.91 Hz, 1H), 7.59 (d, J = 8.23 Hz, 1H), 7.27−7.23 (m, 4H), 7.14−7.12 (m, 5H), 7.05−7.02 (m, 3H), 4.49 (s, 2H), 1.97−1.81 (m, 4H), 1.25−1.04 (m, 66H), 0.87 (t, J = 6.78 Hz, 6H), and 0.72−0.55 (br, 4H); ^{13}C NMR (126 MHz, $CDCl_3$) δ 190.99 (–C=O), 153.63 (aminoaryl carbon), 151.06 (aminoaryl carbon), 148.81 (aminoaryl carbon), 147.61, 146.89, 133.96, 131.55, 129.25, 128.80, 124.36, 123.09, 122.78, 121.61, 118.82, 118.20, 55.23, 39.96, 31.90, 31.15, 29.90, 29.67, 29.64, 29.62, 29.57, 29.55, 29.34, 29.29, 23.83, 22.67, and 14.10.

*Synthesis of 7-(1,2-dihydro-1,2-methano[60]fullerene-61-carbonyl)-9,9-dioctadecyl-2-diphenylaminofluorene, C_{60}(>DPAF-C_{18}) (**1**).* To a mixture of C_{60} (0.75 g, 1.1 mmol) and 7-α-bromoacetyl-9,9-dioctadecanyl-2-diphenylaminofluorene **8** (BrDPAF-C_{18}, 0.85 g, 1.1 mmol) in dry toluene (500 mL) was added DBU (0.18 ml, 1.2 mmol) under a nitrogen atmosphere. After stirring at room temperature for 5.0 h, suspended solids of the reaction mixture were filtered off and the filtrate was concentrated to a 10% volume. Crude product was precipitated by the addition of methanol and isolated by centrifugation (8000 rpm, 20 min). The isolated solid was found to be a mixture of the monoadduct and its bisadducts. Separation of these two product fractions were made by column chromatography (silica gel) using a solvent mixture of hexane−toluene (3:2) as the eluent. The first chromatographic band corresponding to R_f = 0.7 on TLC (SiO_2, hexane−toluene, 3:1) afforded C_{60}(>DPAF-C_{18}) **1** as brown solids (1.12 g, 65% yield based on recovered C_{60}). Spectroscopic data: FT-IR (KBr) ν_{max} 3440 (m), 2920 (s), 2849 (s), 1674 (–C=O, m), 1632 (m), 1593 (s), 1491 (m), 1463 (m), 1427 (m), 1346 (w), 1331 (w), 1316 (w), 1273 (m), 1239 (w), 1200 (m), 1186 (w), 1157 (w), 1028 (w), 817 (w), 752 (m), 738 (w), 696 (m), 575 (w), 547 (w), 526 (m), and 490 (m) cm^{-1}; MALDI-MS (TOF) *m/z* 1598 calculated for $^{12}C_{123}{}^{1}H_{91}{}^{14}N_1{}^{16}O_1$; found, *m/z* 1601, 1600 (MH^+), 1599, 866, 839, 762, 734, and 720; UV-vis ($CHCl_3$) λ_{max} (ε) 260 (1.3×10^5), 325 (4.7×10^4), and 411 (3.6×10^4 L/mol-cm) ^{1}H NMR (500 MHz, $CDCl_3$, ppm) δ 8.43 (d, J = 6.9 Hz, 1H), 8.32 (s, 1H), 7.78 (d, J = 8.0 Hz, 1H), 7.61 (d, J = 8.0 Hz, 1H), 7.25−7.22 (m, 4H), 7.11−7.09 (m, 5H), 7.03−7.00 (m, 3H), 5.66 (s, 1H), 2.03−1.84 (m, 4H), 1.29−1.04 (m, 58H), 0.87 (t, J = 6.88 Hz , 6H), and 0.69 (br, 4H). ^{13}C NMR (126 MHz, $CDCl_3$) δ 188.33 (–C=O), 153.55 (aminoaryl carbon), 151.20 (aminoaryl carbon), 148.77 (aminoaryl carbon), 147.96 (2C), 147.30 (2C), 147.20 (C), 146.73 (2C), 145.35 (2C), 145.24 (2C), 145.06 (2C), 144.96 (4C), 144.85 (2C), 144.70 (C), 144.52 (2C), 144.43 (4C), 144.13 (2C), 143.74 (2C), 143.49 (2C), 143.14 (2C), 142.96 (C), 142.91 (C), 142.83 (2C), 142.76 (2C), 142.57 (2C), 142.32 (2C), 142.07 (2C), 142.00 (2C), 141.90 (2C), 141.06 (2C), 140.76 (2C), 139.36 (2C), 136.46 (2C), 133.57, 133.22, 129.22, 128.62, 124.40, 123.15, 122.83, 122.42, 121.71, 119.14, 117.78, 72.48 (fullerenyl sp^3 carbons), 55.09, 44.58, 40.14 (cyclopropanyl C_{60}> carbon), 32.00, 30.16, 29.81, 29.56, 29.47, 24.11, 22.87, and 14.22. A total of 30 carbon peaks were accounted for 58 fullerenyl sp^2 carbons at δ 136–148 indicated a C_2-symmetry of the fullerene cage.

*Synthesis of 7-[2-bromo-1-(1,1-dicyanoethylenyl)-1-methyl]-9,9-di(2-dimethoxyethyl)-2-diphenylaminofluorene, BrCPAF-C_{2M} (**9**).* To a mixture of 7-α-bromoacetyl-9,9-di(2-methoxyethyl)-2-diphenylaminofluorene **7** (BrDPAF-C_{2M}, 2.17 g, 3.8 mmol) and malononitrile (0.29 g, 4.4 mmol) in dry chloroform (100 mL) was added pyridine (3.0 mL) while stirring under a nitrogen atmosphere. To this solution, titanium tetrachloride (1.0 mL, excess) was added in. After stirring at room temperature for 5.0 min, the reaction mixture was quenched with water (90 mL). The resulting organic layer was washed several times with water (100 mL each), dried over magnesium sulfate, and concentrated *in vacuo* to afford the crude orange-red oil. It was purified on a preparative chromatographic plate (PTLC, SiO_2, $CHCl_3$ as the eluent). A product fraction collected at R_f = 0.6 [toluene−ethyl acetate (4:1) as the eluent] gave BrCPAF-C_{2M} **9** in 89 % yield (2.1 g). Spectroscopic data: FT-IR (KBr) ν_{max} 3058 (w), 3035 (w), 2924 (m), 2870 (m), 2855 (m), 2809 (w), 2226 (m), 1593 (s), 1547 (m), 1490 (s), 1468 (m), 1451 (w), 1384 (w), 1346 (m), 1318 (m), 1279 (s), 1191 (w), 1113 (m), 1028 (w), 957 (w), 821 (w), 755 (m), 698 (m), and 511 (w) cm^{-1}; UV-vis ($CHCl_3$) λ_{max} (ε) 316 (2.1×10^4) and 489 (1.7×10^4 L/mol-cm); ^{1}H NMR (500 MHz, $CDCl_3$, ppm) δ 7.70−7.66 (m, 3H), 7.59 (d, J = 8.3 Hz, 1H), 7.30−7.27 (m, 4H), 7.15−7.13 (m, 5H), 7.09−7.06 (m, 3H), 4.61 (s, 2H), 3.03 (s, 6H), 2.87−2.77 (m, 4H), and 2.32−2.18 (m, 4H); ^{13}C

NMR (126 MHz, $CDCl_3$) δ 170.85 [–C=C(CN)$_2$], 151.77 (aminoaryl carbon), 149.91 (aminoaryl carbon), 149.38 (aminoaryl carbon), 147.28, 145.72, 132.39, 130.13, 129.36, 127.92, 124.74, 123.54, 122.91, 122.55, 121.72, 119.60, 117.55, 112.98 (–C≡N), 112.11 (–C≡N), 84.48 [=C(CN)$_2$], 68.42, 58.31, 51.64, 38.93, and 28.68.

Synthesis of 7-(1,2-dihydro-1,2-methano[60]fullerene-61-{1,1-dicyanoethylenyl})-9,9-di(2-methoxyethyl)-2-diphenylaminofluorene, C_{60}(>CPAF-C_{2M}) (2). To a mixture of C_{60} (0.18 g, 0.25 mmol) and 7-[2-bromo-1-(1,1-dicyanoethylenyl)-1-methyl]-9,9-di(2-methoxyethyl)-2-diphenylaminofluorene **9** (BrCPAF-C_{2M}, 0.15 g, 0.24 mmol) in dry toluene (150 mL) was added 1,8-diazabicyclo[5,4,0]-undec-7-ene (DBU, 0.1 M, 2.6 mL) under a nitrogen atmosphere. After stirring at room temperature for a period of 5.0 h, the reaction mixture was concentrated to a volume of approximately 10 mL. Crude product was precipitated by the addition of methanol and isolated by centrifugation (8000 rpm, 20 min). The precipitate was further purified by column chromatography [silica gel, toluene−ethyl acetate (4:1) as the eluent] at the corresponding chromatographic R_f = 0.8 on TLC (SiO_2) with the same eluent to afford C_{60}(>CPAF-C_{2M}) **2** in 53% yield (0.16 g). Spectroscopic data: FT-IR (KBr) ν_{max} 3439 (s), 2980 (w), 2920 (m), 2868 (m), 2824 (w), 2798 (w), 2224 (–C≡N, m), 1629 (m), 1594 (vs), 1538 (m), 1491 (m), 1466 (m), 1428 (m), 1347 (m), 1319 (m), 1279 (s), 1186 (m), 1115 (m), 1028 (w), 958 (w), 888 (w), 820 (m), 805 (w), 754 (m), 697 (m), 668 (w), 577 (w), and 527 (m) cm^{-1}; MALDI-MS (TOF) *m/z* 1257 calculated for $^{12}C_{96}{}^{1}H_{31}{}^{14}N_3{}^{16}O_2$; found, *m/z* 1260, 1259, 1258 (MH^+), 1155, 987, 965, 919, 735, and 720; UV-vis ($CHCl_3$) λ_{max} (ε) 260 (1.2×10^5), 327 (5.1×10^4), and 501 nm (1.7×10^4 L/mol-cm); ^{1}H NMR (500 MHz, $CDCl_3$, ppm) δ 8.14 (d, J = 8.2 Hz, 1H), 8.11 (s, , 1H), 7.76 (d, J = 7.97 Hz, 1H), 7.56 (d, J = 7.97 Hz, 1H), 7.26−7.23 (m, 4H), 7.09−7.08 (m, 5H), 7.06−7.03 (m, 3H), 5.51 (s, 1H), 2.95 (s, 6H), 2.73 (t, J = 7.97 Hz, 4H), and 2.32−2.18 (m, 4H); ^{13}C NMR (126 MHz, $CDCl_3$) δ 167.64 [–C=C(CN)$_2$], 151.83 (aminoaryl carbon), 150.31 (aminoaryl carbon), 149.45 (aminoaryl carbon), 147.23 (2C), 147.06 (2C), 146.07 (C), 145.69 (2C), 145.25 (4C), 145.21 (2C), 145.18 (2C), 145.15 (2C), 145.03 (2C), 144.72 (4C), 144.68 (4C), 144.53 (2C), 144.40 (2C), 144.15 (C), 143.69 (2C), 143.62 (2C), 142.94 (2C), 142.89 (4C), 142.36 (2C), 141.96 (2C), 141.94 (2C), 141.83 (2C), 141.36 (2C), 140.97 (2C), 137.31 (2C), 136.95 (2C), 132.12, 129.36, 128.46, 124.76, 123.63, 122.89, 122.39, 121.89, 119.67, 117.47, 112.99 (–C≡N), 112.92, 88.07 [=C(CN)$_2$], 72.30 (fullerenyl sp^3 carbons), 68.33, 58.26, 51.56, 41.22 (cyclopropanyl C_{60}> carbon), and 39.26. A total of 30 carbon peaks representing 58 fullerenyl sp^2 carbons at δ136–148 indicated a C_2-symmetry of the fullerene cage.

*Synthesis of hybrid [(9,9-dioctadecyl-2-diphenylaminofluorenyl)-7-carbonyl]-{[9,9-(2-dimethoxyethyl)-2-diphenylaminofluorenyl]-7-(1,1-dicyanoethylenyl)}-bis(1,2-dihydro-1,2-methano)[60]fullerenyl triad C_{60}(>DPAF-C_{18})(>CPAF-C_{2M}) (**3**) and its tetrad analogous C_{60}(>DPAF-C_{18})(>CPAF-C_{2M})$_2$ (**4**).* To the mixture of 7-(1,2-dihydro-1,2-methano[60]fullerene-61-carbonyl)-9,9-di(octadecyl)-2-diphenylaminofluorene C_{60}(>DPAF-C_{18}) **1** (0.48 g, 0.3 mmol) and 7-[2-bromo-1-(1,1-dicyanoethylenyl)-1-methyl]-9,9-di(2-methoxyethyl)-2-diphenylaminofluorene **9** (BrCPAF-C_{2M}, 0.37 g, 0.6 mmol) in dry toluene (100 mL) was added 1,8-diazabicyclo[5,4,0]-undec-7-ene (DBU, 0.1 M, 6.0 mL) slowly under a nitrogen atmosphere. After stirring at room temperature for a period of 5.0 h, the reaction mixture was concentrated to a volume of approximately 10 mL. Crude product was precipitated by the addition of methanol and isolated by centrifugation (8000 rpm, 20 min). The isolated solid was found to be a mixture of the fullerene multiadducts. Separation of these mixture was made by column chromatography (silica gel) using a solvent mixture of toluene–ethyl acetate (9:1) as the eluent. The first chromatographic band gave the unreacted starting compound 1 (0.08 g, 0.05 mmol). The second chromatographic band corresponding to R_f = 0.5 on the thin-layer chromatographic plate [TLC, SiO_2, toluene–ethyl acetate (9:1) as the eluent] afforded the bisadduct product C_{60}(>DPAF-C_{18})(>CPAF-C_{2M}) **3** as orange-brown solids (0.15 g, 0.07 mmol) in a 28% yield [based on the recovered C_{60}(>DPAF-C_{18}) amount]. The third chromatographic band corresponding to R_f = 0.4 on the thin-layer chromatographic plate [TLC, SiO_2, toluene-ethyl acetate (4:1) as the eluent] afforded the trisadduct product C_{60}(>DPAF-C_{18})(>CPAF-C_{2M})$_2$ **4** as red-brown solids (0.28 g, 0.10 mmol) in a yield of 40% [based on the recovered C_{60}(>DPAF-C_{18}) amount]. Spectroscopic data of C_{60}(>DPAF-C_{18})(>CPAF-C_{2M}) **3**: FT-IR (KBr) ν_{max}

3424 (w), 3063 (w), 3030 (w), 2921 (m), 2850 (m), 2223 (m), 1678 (m), 1593 (s), 1568 (m), 1537 (w), 1492 (m), 1465 (m), 1426 (m), 1346 (m), 1277 (s), 1202 (m), 1115 (m), 1074 (w), 962 (w), 895 (w), 819 (m), 753 (s), 696 (s), 578 (w), 526 (m), and 491 (w) cm^{-1}; MALDI-MS (TOF) *m/z* 2135 calculated for $^{12}C_{159}{}^{1}H_{122}{}^{14}N_4{}^{16}O_3$; found, *m/z* 2136 ($MH^+$), 2135 ($M^+$), 965, 920, 866, 763 {$C_{60}$[>(C=O)-H]$H^+$}, 735 ($C_{60}$>$H^+$), and 720 ($C_{60}{}^+$); UV-vis ($CHCl_3$) λ_{max} (ε) 255 (1.1×10^5), 304 (7.5×10^4), 413 (3.9×10^4), and 494 nm (2.3×10^4 L/mol-cm); ^{1}H NMR (500 MHz, $CDCl_3$, ppm) δ 8.51−7.52 (m, 8H), 7.28−7.22 (m, 8H), 7.14−7.00 (m, 16H), 5.76−5.18 (m, 2H), 3.01−2.90 (br, 6H), 2.82−2.67 (br, 4H), 2.40−2.14 (br, 4H), 2.06−1.80 (br, 4H), 1.31−1.04 (m, 58H), 0.87 (t, J = 6.72 Hz , 6H), and 0.67 (br, 4H).

Spectroscopic data of C_{60}(>DPAF-C_{18})(>CPAF-C_{2M})$_2$ **4**: FT-IR (KBr) ν_{max} 3433 (m), 3060 (w), 3027 (w), 2922 (m), 2851 (m), 2224 (m), 1679 (w), 1594 (s), 1539 (w), 1492 (s), 1466 (m), 1426 (m), 1346 (m), 13317 (w), 1279 (s), 1207 (w), 1115 (m), 1028 (w), 958 (w), 892 (w), 818 (m), 753 (m), 697 (m), 616 (w), and 525 (w) cm^{-1}; MALDI-MS (TOF) *m/z* 2672 calculated for $^{12}C_{195}{}^{1}H_{153}{}^{14}N_7{}^{16}O_5$; found, *m/z* 2673 ($MH^+$), 2672 ($M^+$), 965, 920, 866, 763 {$C_{60}$[>(C=O)-H]$H^+$}, 735 ($C_{60}$>$H^+$), and 720 ($C_{60}{}^+$); UV-vis ($CHCl_3$) λ_{max} (ε) 304 (1.1×10^5), 417 (4.6×10^4), and 500 nm (4.6×10^4 L/mol-cm); ^{1}H NMR (500 MHz, $CDCl_3$, ppm) δ 8.44−7.46 (m, 16H), 7.09−7.03 (br, 32H), 5.57−4.72 (m, 3H), 3.08−2.86 (br, 12H), 2.73 (br, 8H), 2.21 (br, 8H), 1.91 (br, 4H), 1.3−0.95 (m, 58H), 0.86 (t, J = 6.55 Hz , 6H), and 0.64 (br, 4H).

3.3 Spectroscopic Measurements

Infrared spectra were recorded as KBr pellets on a Thermo Nicolet Avatar 370 FT-IR spectrometer. ^{1}H NMR and ^{13}C NMR spectra were recorded on a Bruker Avance Spectrospin–500 spectrometer. UV-vis spectra were recorded on a Perkin Elmer Lambda 750 UV-vis-NIR Spectrometer. Photoluminescence (PL) spectra were measured using PTI Fluorescence Master Systems connected with a photomultiplier (914 Photomultiplier Detection System) with Xenon short arc lamp as the excitation source. Mass spectroscopic measurements were performed by the use of positive ion matrix-assisted laser desorption ionization (MALDI–TOF) technique on a micromass M@LDI-LR mass spectrometer. The sample blended or dissolved in the matrix material was irradiated by nitrogen UV laser at 337 nm with 10 Hz pulses under high vacuum. Mass ion peaks were identified for the spectrum using the MassLynx v4.0 software. In a typical experiment, the samples of C_{60}(>DPAF-C_{18}), C_{60}(>CPAF-C_{2M}), C_{60}(>DPAF-C_{18})(>CPAF-C_{2M}), or C_{60}(>DPAF-C_{18})(>CPAF-C_{2M})$_2$ were dissolved in $CHCl_3$ in a concentration of 1.0 mg/mL. The matrix of 3,5-dimethoxy-4-hydroxycinnamic acid (sinapic acid) was dissolved in THF in a concentration of 10 mg/mL. The solution of matrix (1.0 mL) was taken and mixed with the sample solution (0.1 mL) prior to the deposition on a stainless-steel MALDI target probe. It was subsequently dried at ambient temperature. The blended sample or dissolved in the matrix material was irradiated by nitrogen UV laser at 337 nm with 10 Hz pulses under high vacuum. Mass ion peaks were identified for the spectrum using the MassLynx v4.0 software.

3.4. *Z*-scan and Light-Intensity-Dependent Transmittance Measurements

Z-scan measurements and irradiance-dependent transmission measurements were carried out at the wavelength of either 780 or 980 nm using 125-fs laser pulses with the repetition rate of 1.0 kHz. Laser pulses were generated by an optical parametric amplifier system (TOPAS) pumped by a Ti-Sapphire regenerative amplifier (Spitfire Pro, Spectra Physics/Newport) and focused onto a 1.0-mm thick quartz cuvette containing a solution of methano[60]fullerene derivatives. Incident and transmitted laser intensities were monitored as the cuvette was moved (or *Z*-scanned) along the propagation direction of the laser pulses. The data sets were normalized to the linear transmittance and sample inhomogeneities for all *Z*-scans by the correction of the background transmittance, $T(|Z|- Z_o)$. Total absorption was described by the change in the absorption coefficient $\Delta\alpha = \beta I$, where β and I are the 2PA coefficient and the light intensity, respectively. The absorption coefficient could be extracted from the line fitting between the *Z*-scan theory and the data. The 2PA cross-section value was then calculated from the coefficient by the formula $\sigma_2 = \beta\hbar\omega/N$, where $\hbar\omega$ is the photon energy and N is the number of the molecules.

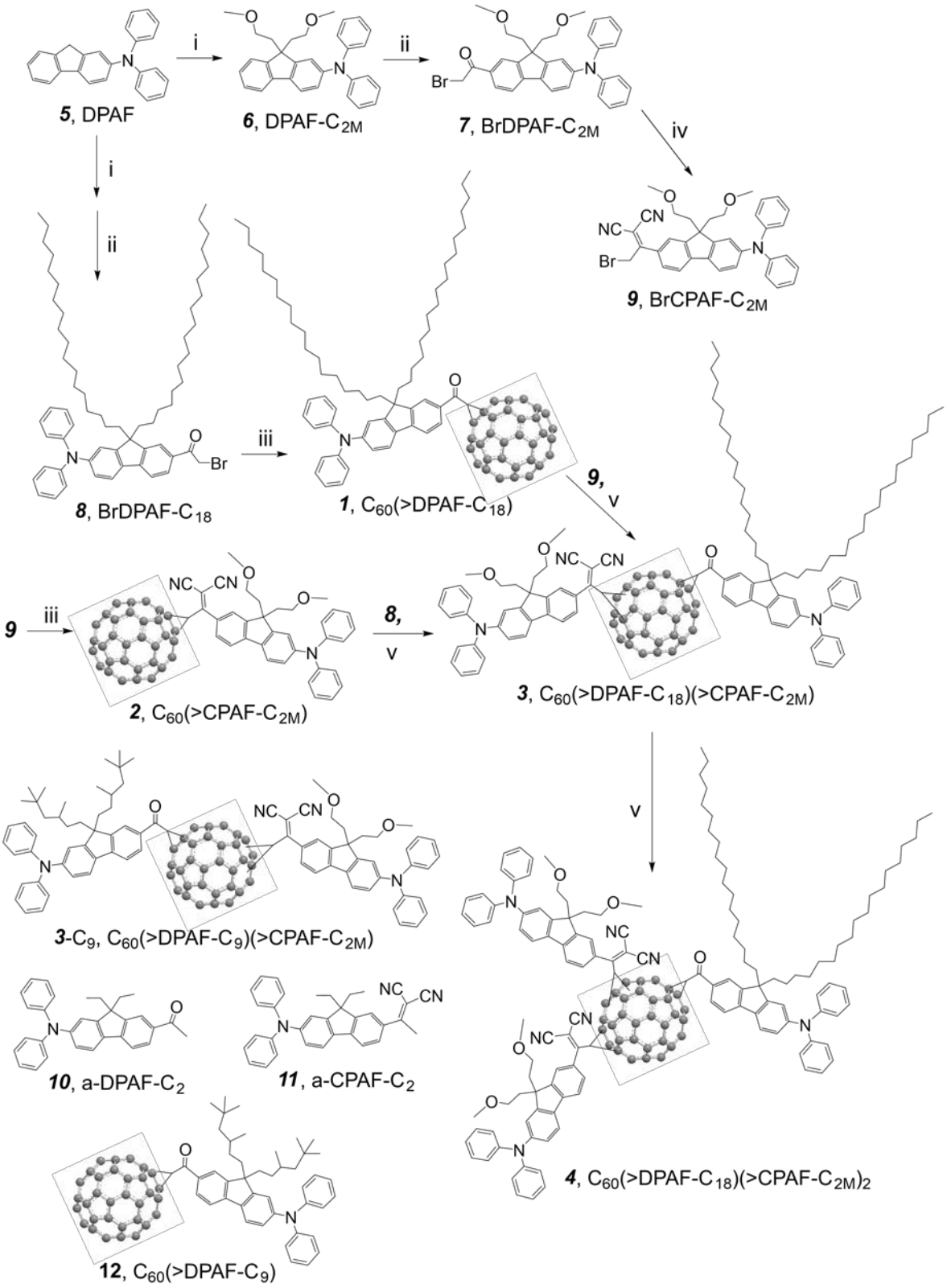

Scheme 1. Synthesis of hybrid C_{60}-(antenna)$_x$ nanostructures **3**, **3**-C_9, and **4**. Reagent and reaction conditions: i. 2-MeOCH_2CH_2–OMs (for **6**), 1-$C_{18}H_{37}$Br (for **8**), *t*-BuOK in THF, 0 ^oC–r.t., 4 h; ii. bromoacetyl bromide, $AlCl_3$, $ClCH_2CH_2Cl$, 0 ^oC, 4 h; iii. C_{60}, DBU, toluene, r.t., 4 h; iv. $TiCl_4$, pyridine, $CH_2(CN)_2$, $CHCl_3$, r.t., 5.0 min; v. DBU, toluene, r.t., 4 h.

4.0 RESULTS AND DISCUSSION

4.1 Synthesis and Material Characterization by Spectroscopic Methods

Structural design of hybrid [60]fullerene triads and tetrads was based on both linear and nonlinear optical characteristics of 9,9-dioctadecyl-2-diphenylaminofluorenyl-61-carbonylmethano[60]fullerene **1**, C_{60}(>DPAF-C_{18}),[42] and 9,9-di(2-methoxyethyl)-2-diphenylaminofluorenyl-61-(1,1-dicyanoethylenyl)-methano[60]fullerene **2**, C_{60}(>CPAF-C_{2M}),[32] to construct an unique nanostructure system with a shared C_{60} cage. Specifically, covalent attachment of an antenna donor chromophore to a C_{60} molecule (electron-acceptor) was accomplished via a periconjugation linkage with a physical separation distance of only <3.5 Å between the donor and acceptor moieties. This led to the realization of ultrafast intramolecular energy- and/or electron-transfer from photoexcited antenna moiety to C_{60} in <130–150 fs[15] that made this type of C_{60}-antenna conjugates, C_{60}(>DPAF-C_n)$_x$, capable of exhibiting photoresponse in a nearly instantaneous time scale to protect against high-intensity radiation. By increasing the number of attached antennae to four per C_{60} cage giving *starburst* pentad nanostructures, highly enhanced fs 2PA cross-section values were observed in a concentration-dependent manner.[31] Upon the chemical alteration of the keto group of C_{60}(>DPAF-C_n) bridging between C_{60} and the antenna moiety to a highly electron-withdrawing 1,1-dicyanoethylenyl (DCE) group, it was possible to extend the π-conjugation in the resulting C_{60}(>CPAF-C_n) analogous chromophore molecules to a close contact with the cage current. This led to a large bathochromic shift of the linear optical absorption of C_{60}(>CPAF-C_2) moving from 410 nm (λ_{max}) of the parent keto-compound to 503 nm with the shoulder band being extended beyond 550 nm in the UV-vis spectrum. The shift considerably increased its light-harvesting ability in visible wavelengths and caused a nearly 6-fold higher in the production quantum yield of singlet oxygen ($^1O_2$) from C_{60}(>CPAF-C_{2M}) as compared with that of C_{60}(>DPAF-C_{2M}). The mechanism of $^1O_2$ production was originated from the intermolecular triplet-energy transfer from the ^{3}(C_{60}>)* cage moiety to $^3O_2$. A large increase in the production of reactive oxygen species (ROS) by excited C_{60}(>CPAF-C_{2M}) explained its effective photokilling of HeLa cells in vitro, via 1γ-PDT.[32] The observation demonstrated the intramolecular/intramolecular interaction between the excited CPAF-C_n donor antenna moiety and the acceptor C_{60} cage that was also confirmed by transient absorption spectroscopic measurements using ns laser pulses at 480–500 nm.[33] The behavior resembles that of DPAF-C_n antenna with transient photoexcitation at 380–410 nm reported previously.[34] By extending the same intramolecular photophysical properties to 2PA-based excitation applications, these C_{60}-(antenna)$_x$ analogous nanostructures may be utilized as potential photosensitizers for 2γ-PDT at either 800 nm (with DPAF antenna) or 1000 nm (with CPAF antenna) that is well-suited to the biological optical window of 800–1100 nm.

Accordingly, selective attachment of these two antenna moiety types DPAF-C_n and CPAF-C_n in combination as hybrid chromophore addends to a single C_{60} cage should result in the formation of new methano[60]fullerene triads, C_{60}(>DPAF-C_{18})(>CPAF-C_{2M}) **3**, and tetrads, C_{60}(>DPAF-C_{18})(>CPAF-C_{2M})$_2$ **4**, as shown in Scheme 1. The core chromophore moiety of **3** and **4** will then be capable of performing dual-band 2γ-PDT-based photoinduced biocidal effects with enhanced penetration depth at 800–1100 nm. Synthetically, preparation of 3 and 4 was accomplished by the synthesis of a structurally well-defined monoadduct 1 followed by the attachment of one or two CPAF-C_{2M} antenna in sequence. A key intermediate precursor, 7-α-bromoacetyl-9,9-dioctadecyl-2-diphenylaminofluorene 8, BrDPAF-C_{18}, was prepared by a three-step reaction involving first palladium catalyzed diphenylamination of commercially available 2-bromofluorene at the C2 position of the fluorene ring to afford DPAF 5 (Scheme1). It was followed by dialkylation at the C9 carbon position of **5** using 1-bromooctadecane as the reagent in the presence of potassium *t*-butoxide, as a base, in THF at 0–25 °C to give the corresponding 9,9-dioctadecyl-2-diphenylaminofluorene (DPAF-C_{18}) in 97% yield. Friedel Crafts acylation of DPAF-C_{18} with α-bromoacetyl bromide and $AlCl_3$ in CH_2Cl-CH_2Cl at 0 °C for a period of 4.0 h afforded the compound 8 in a yield of 96%. Addition reaction of **8** to C_{60} was carried out in the presence of 1,8-diazabicyclo[5.4.0]undec-7-ene (DBU, 1.0 eq.) at ambient temperature for 4.0 h to result

in C_{60}(>DPAF-C_{18}) **1** in 65% yield (based on recovered residual C_{60}) after column chromatographic purification.

A similar reaction sequence was applied for the synthesis of the compound **2** by replacing two octadecyl groups with 2-methoxyethyl groups. Thus, 2-methoxyethyl methanesulfonate was used as a leaving group for dialkylation of DPAF **5** followed by Friedel Crafts acylation with *α*-bromoacetyl bromide and $AlCl_3$ to yield 7-*α*-bromoacetyl-9,9-di(2-methoxy)ethyl-2-diphenylaminofluorene **7**, BrDPAF-C_{2M}. Subsequent conversion of the keto group of **7** to the corresponding 1,1-dicyanoethylenyl (DCE) group was carried out by the reaction using malononitrile as a reagent, pyridine as a base, and titanium tetrachloride as a deoxygenation agent in dry chloroform at ambient temperature for a short period of 5.0 min. The reaction resulted in the corresponding diphenylaminofluorene BrCPAF-C_{2M} **9** in a yield of 89% after chromatographic (PTLC, SiO_2, $CHCl_3$ as the eluent) purification. Attachment of a CPAF-C_{2M} antenna arm to a C_{60} cage was carried out by identical reaction conditions as those for **1** with DBU (1.0 eq.) at room temperature for 4.0 h to afford 7-(1,2-dihydro-1,2-methano[60]fullerene-61-{1,1-dicyanoethylenyl})-9,9-di(2-methoxyethyl)-2-diphenylaminofluorene **2**, C_{60}(>CPAF-C_{2M}), as orange red solids in 53% yield (based on recovered C_{60}). The bulkiness of DPAF-C_{18} and CPAF-C_{2M} in size can prevent these two types of antenna moieties form locating in close vicinity to each other at the cage surface. By considering the regio-location of reactive bicyclopentadienyl olefin bonds on the fullerene surface, when the first antenna is bound at the north-pole location, the second antenna arm is most likely to be pushed away to the equator area of the C_{60} sphere. Therefore, only a very limited number of multiadduct regioisomers per C_{60} are likely to form. Indeed, by controlling the reaction kinetic rate with two molar equivalents of CPAF-C_{2M} applied in the reaction with 1 in the presence of DBU (2.0 eq.), only two clear PTLC (SiO_2, toluene–ethyl acetate/9:1 as the eluent) bands in the product mixtures were observed in addition to the starting **1** (~15%). The first less polar product band at R_f = 0.5 was found to be the bisadduct C_{60}(>DPAF-C_{18})(>CPAF-C_{2M}) **3** isolated as orange-brown solids in 28% yield. The second more polar product band at R_f = 0.4 (toluene–ethyl acetate/4:1 as the eluent) was determined to be the trisadduct C_{60}(>DPAF-C_{18})(>CPAF-C_{2M})$_2$ **4** isolated as red-brown solids in 40% yield.

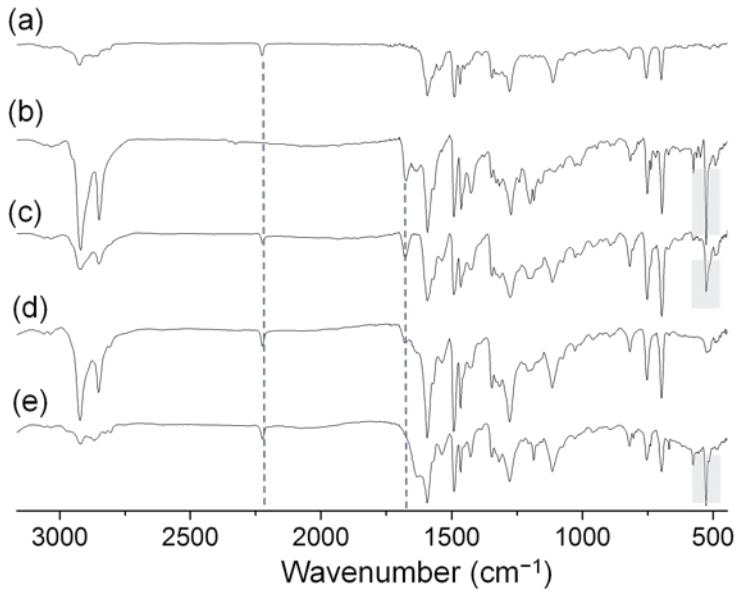

Figure 1. Infrared spectra of (a) BrCPAF-C_{2M} **9**, (b) C_{60}(>DPAF-C_{18}) **1**, (c) C_{60}(>DPAF-C_{2M})(>CPAF-C_{2M}) **3**, (d) C_{60}(>DPAF-C_{18})(>CPAF-C_{2M})$_2$ **4**, and (e) C_{60}(>CPAF-C_{2M}) **2**.

Spectroscopic characterization of **1** and **2** was performed mainly by (i) the clear detection of a group of molecular mass ion peaks with the maximum peak intensity centered at *m/z* 1600 (MH^+ of 1) and 1258 (MH^+ of 2) (supporting information) using positive ion matrix-assisted laser desorption ionization (MALDI–TOF) mass spectroscopy and (ii) analyses of ^{13}C NMR spectra. The former spectra

were also accompanied with two groups of fragmented mass ion peaks at *m/z* 720 and 734/735 corresponding to the mass units of C_{60} and C_{60}>, respectively, indicating high stability of the fullerene cage under MALDI-MS conditions. In addition to the IR spectral analysis (Figure 1) of the carbonyl stretching vibration band at 1674 cm^{-1} for **1** and the cyano (–C≡N) stretching band centered 2224 cm^{-1} for **2**, chemical shifts of a keto carbonyl carbon peak at δ 188.33 and three carbons, –C=C$(CN)_2$, –C≡N, and =C$(CN)_2$, in 1,1-dicyanoethylenyl (DCE) moiety of **2** at δ 167.64, 112.99, and 88.07, respectively, in their ^{13}C NMR spectra (Figures 2b and 2d) clearly consistent with both structures. Chemical shift of the former carbonyl carbon peak agrees well with that of BrDPAF-C_{18} 8 at δ 190.99 (Figure 2a). The δ values of the latter three DCE carbons were also found to match well with those of BrCPAF-C_{2M} 9 (Figure 2c) at δ 170.85, 112.98, (–C≡N), 112.11 (–C≡N), and 84.48, respectively. In the same spectra,

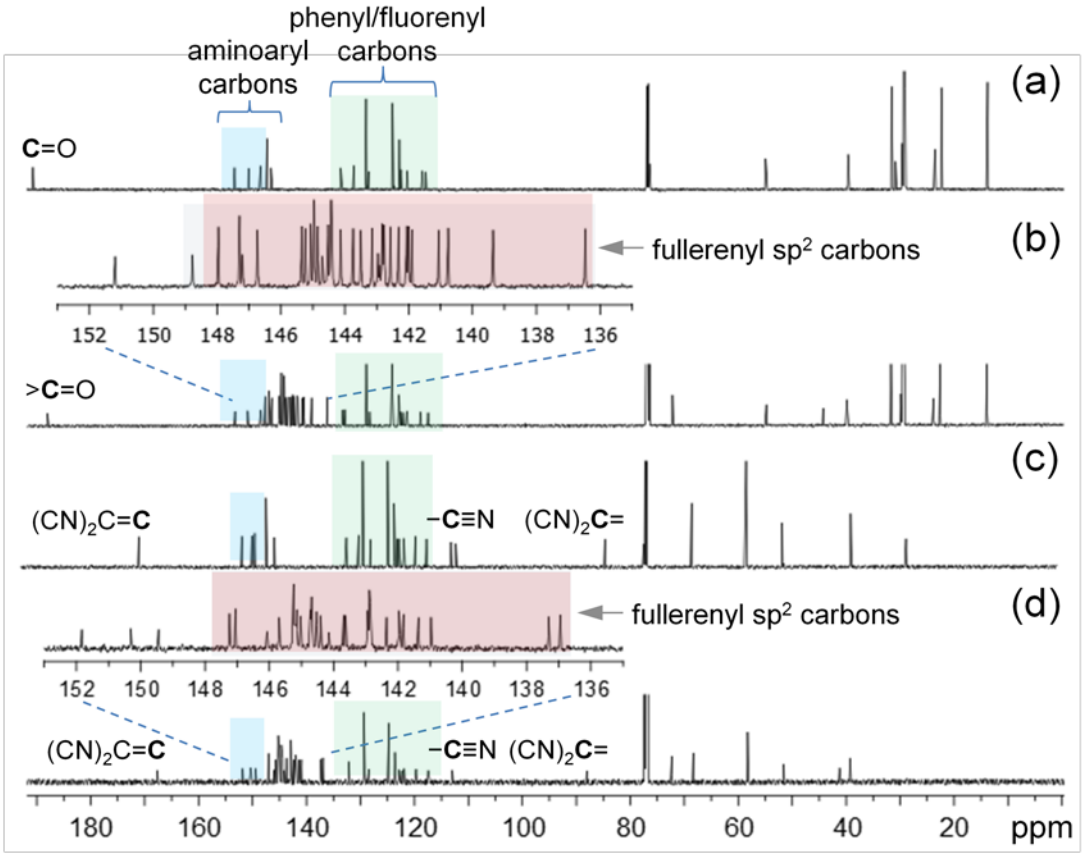

Figure 2. ^{13}C NMR spectra of (a) BrDPAF-C_{18} **8**, (b) C_{60}(>DPAF-C_{18}) **1**, (c) BrCPAF-C_{2M} **9**, and (d) C_{60}(>CPAF-C_{2M}) **2** with three regions of carbon peaks marked by blue, green, and brown.

the peaks at δ 40.14/41.22 and 72.48/72.30 were assigned to the cyclopropanyl or methanofullerene carbon C_{61} (C_{60}>) and fullerenyl sp^3 carbons of 1/2, respectively.

The rest of aromatic carbon peaks were separated from each other into three different groups with assigned chemical shifts of (i) three aminoaryl carbons of 1/2 at δ (153.55, 151.20, 148.77)/(151.83, 150.31, 149.45) in close resemblance to those of **8** and **9**, respectively, (ii) phenyl and fluorenyl carbons at δ 115–135, and (iii) fullerenyl sp^2 carbons located at δ 136–148, as shown in Figure 2. A total of 30 fullerenyl carbon (28 × 2C and 2 × 1C) signals, some with similar or slightly shifted δ, were accounted for 58 sp^2 fullerenyl carbons that fits well with a C_2 molecular symmetry of the compounds **1** and **2**.

With well-characterized structures of **1** and **2**, we were able to utilize their ^{1}H NMR spectra for the correlation and identification of hybrid [60]fullerene triads **3** and tetrads **4**. Upon the attachment of one CPAF-C_{2M} antenna arm to **1**, a new cyano stretching band centered at 2223 cm^{-1} in addition to the carbonyl stretching band at 1678 cm^{-1} were detected as expected. Intensity of characteristic half-

fullerene cage absorption band at ~526 cm^{-1} was found to decrease significantly going from that of **1**, **3**,

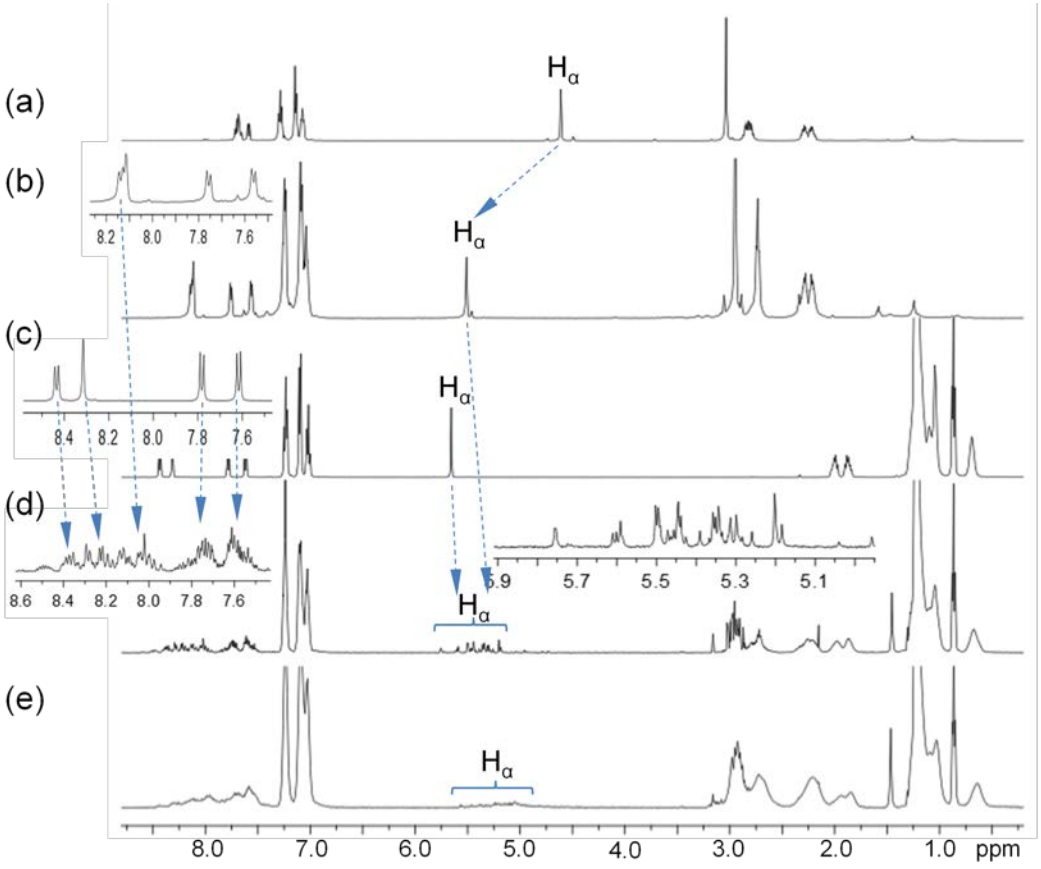

Figure 3. ^{1}H NMR spectra ($CDCl_3$) of (a) BrCPAF-C_{2M} **9**, (b) C_{60}(>CPAF-C_{2M}) **2**, (c) C_{60}(>DPAF-C_{18}) **1**, (d) C_{60}(>DPAF-C_{18})(>CPAF-C_{2M}) **3**, and (e) C_{60}(>DPAF-C_{18})(>CPAF-C_{2M})$_2$ **4**.

to **4** (Figure 1) indicating the increasing percentage of regioisomers having at least one CPAF-C_{2M} addend located at more than 90^o away the DPAF-C_{18} arm (or the other side of the cage surface). Large difference of ^{1}H chemical shifts among alkyl groups of DPAF-C_{18} (methyl and the most of methylene proton peaks at δ 0.69–1.29) and CPAF-C_{2M} (singlet terminal methoxy CH_3-O– proton peak at δ 2.95 and triplet methylenoxy –CH_2-O– proton peaks centered at δ 2.73) allowed us to measure a clear proton integration count to verify the structure of **3** and **4** as a bisadduct and trisadduct, respectively, as shown in Figure 3. A more branched structure of 4 was also evident by the detection of a higher aromatic proton integration ratio in the region of δ 7.5–7.8 and 8.10–8.15 (Figures 3b and 3e) of CPAF moieties. The most distinguishable proton peaks at δ 5.5–5.7 in these spectra were assigned for α-protons each bound on the cyclopropanyl carbon located between either the keto (for DPAF) or DCE (for CPAF) group and the C_{60} cage. Owing to the fullerenyl ring current, a large down-field shift of the δ value was observed at δ 5.66 (for the keto α-H) and 5.51 (for the DCE α-H) from that of the fluorenyl α-bromoketo α-H at δ 4.61 (Figures 3a–c) or δ 2.6 for fluorenyl keto α-H (without α-attachment of a bromine atom, a large shift of ~3.0 ppm). It also caused a down-fielded δ shift of 0.44–0.48 ppm for fluorenyl protons located at the vicinity of C_{60}> moiety that clearly revealed strong electronic interactions between DPAF-C_{18}/CPAF-C_{2M} antenna moieties and the fullerene cage.

A number of α-H peaks were observed in the ^{1}H NMR spectrum of **3** (the inset of Figure 3d). By taking the consideration of four possible different orientational configurations for each regioisomer, as examples shown in Figure 4, one regioisomeric molecule may display four keto α-H_a peaks (from the DPAF-C_{18} moiety) and four DCE α-H_b peaks (from the CPAF-C_{2M} moiety) in the region of δ 5.0–5.75. Therefore, detected α-H_a peaks each in different intensities can be separately grouped into and accounted for two major regioisomer products and one minor regioisomer product. High similarity of molecular

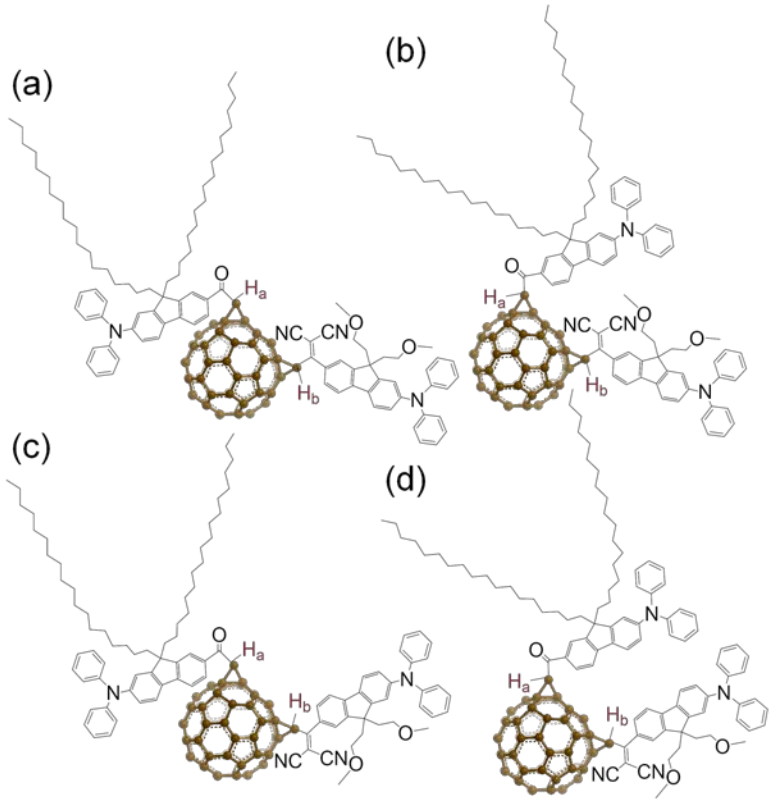

Figure 4. Four possible structural conformers for each regioisomer of C_{60}(>DPAF-C_{18})(>CPAF-C_{2M}) **3**.

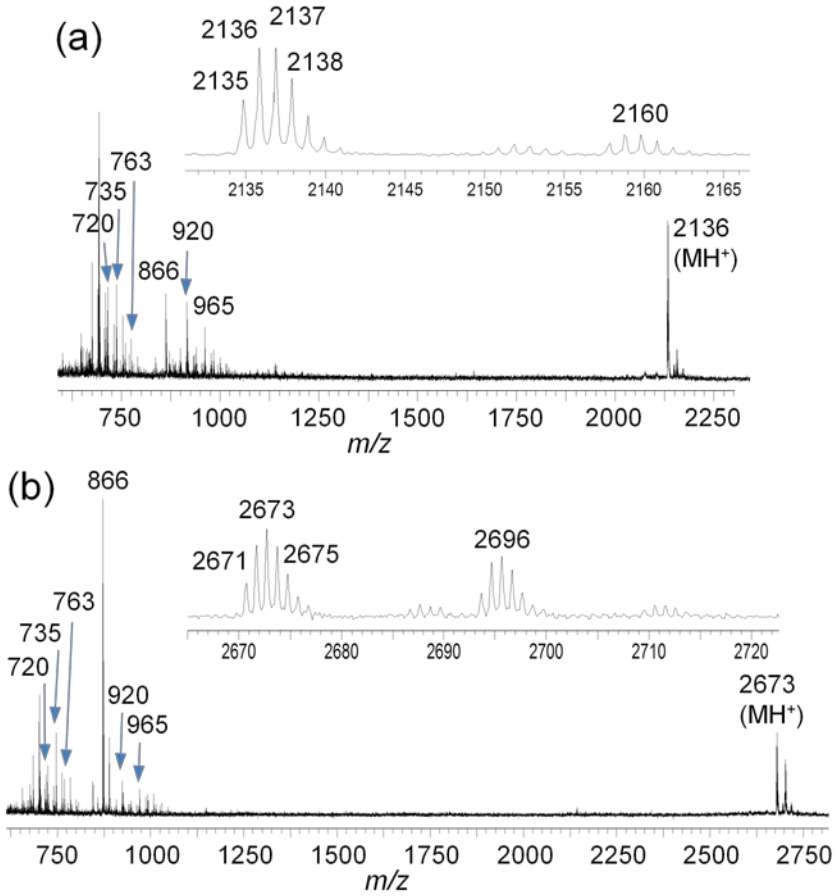

Figure 5. MALDI mass spectra of (a) C_{60}(>DPAF-C_{18})(>CPAF-C_{2M}) **3** and (b) C_{60}(>DPAF-C_{18})(>CPAF-C_{2M})$_2$ **4**.

polarity among these regioisomers prohibited us to separate them chromatographically. However, we were able to confirm the identical composition mass of these regioisomers by detecting an group of sharp molecular mass ions with the maximum mass at *m/z* 2136 (MH^+), as shown in Figure 5a. It was accompanied by a relatively simple MALDI-TOF mass spectrum showing fully fragmented mass ions at *m/z* 763, 735, and 720 corresponding clearly to the mass of $C_{60}[>(C=O)\text{-}H]H^+$, $C_{60}>H^+$, C_{60}^+, respectively, that was consistent well with the molecular structure of triad C_{60}(>DPAF-C_{18})(>CPAF-C_{2M}) 3. In the case of tetrad C_{60}(>DPAF-C_{18})(>CPAF-C_{2M})$_2$ **4**, a group of sharp molecular mass ions with the maximum mass at *m/z* 2673 (MH^+) and similar fragmented mass ions to those of **3** in the low mass region of *m/z* 720–1000 were detected (Figure 5b). These MS data revealed high stability of aromatic diphenylaminofluorene moiety under measurement conditions. Additional high mass groups of peaks with the peak maximum at *m/z* 2160 of Figure 5a and *m/z* 2696 of Figure 5b are satellite peaks with an increase of 2C (*m/z* 24) mass from those of molecular ion mass peaks, as common phenomena for fullerenyl nanocarbon materials, especially, under the high laser power conditions used for the collection of high mass ions. The fragmentation pattern fits well with the bond cleavage occurring mostly at the cyclopropanyl carbon bonds bridging the C_{60} cage and DPAF-C_{18}/CPAF-C_{2M} antenna moiety. The overall spectra provided strong evidence for the mass composition of **3** and **4**.

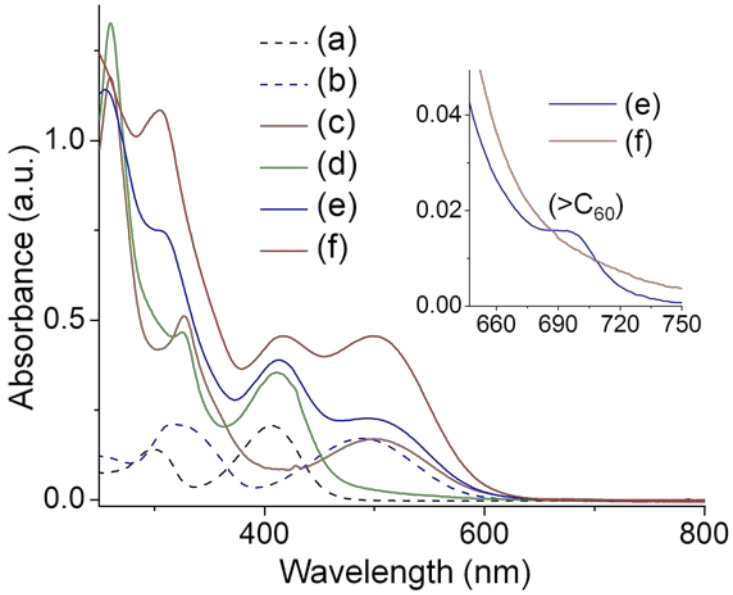

Figure 6. UV-vis spectra of (a) BrDPAF-C_{18} **8**, (b) BrCPAF-C_{2M} **9**, (c) C_{60}(>CPAF-C_{2M}) **2**, (d) C_{60}(>DPAF-C_{18}) **1**, (e) C_{60}(>DPAF-C_{18})(>CPAF-C_{2M}) **3**, (f) C_{60}(>DPAF-C_{18})(>CPAF-C_{2M})$_2$ **4**, in chloroform at a concentration of 1.0×10^{-5} M.

Optical absorption of **1** and **2** (Figures 6d and 6c, respectively) was characterized by two distinguishable bands centered at 260 and 325–327 nm both arising from the C_{60}> cage moiety that agrees with allowed $^1T_{1u} \rightarrow {}^1A_g$ transition bands of pristine C_{60}.[43] The third band with λ_{max} at either 411 or 501 nm for **1** or **2**, respectively, matches approximately with those of the corresponding precursor compound BrDPAF-C_{18} (Figure 6a) or BrCPAF-C_{2M} (Figure 6b). These bands are in the characteristic photoresponsive wavelength range of DPAF-C_{18} or CPAF-C_{2M} antenna, respectively. When these two types of antenna were simultaneously attached to the same C_{60} in 3, two absorption bands with λ_{max} (ε) at 413 (3.9×10^4) and 494 nm (2.3×10^4 L/mol-cm) were observed in the spectrum showing extinction coefficient ε values matching roughly with those of 1 and 2. This clearly revealed a 1:1 ratio of DPAF-C_{18}/CPAF-C_{2M} in **3** consistent with its composition. As the number of CPAF-C_{2M} antenna being increased to two in **4**, the corresponding two bands remained in the same range with λ_{max} (ε) at 417 (4.6×10^4) and 500 nm (4.6×10^4 L/mol-cm). The extinction coefficient ε value of the second band is nearly double to that of **3**. The structural modification resulted in approximately equal visible absorption in intensity over the full wavelength range of 400–550 nm. Accordingly, these bands can be utilized for the

corresponding near-IR two-photon absorption excitation at 800–1100 nm, giving broadband characteristics of the materials while exhibiting good linear transparency beyond 800 nm (Figures 6e and 6f). In the long-wavelength absorption region beyond 650 nm, a very weak characteristic steady-state absorption band of methano[60]fullerene (C_{60}>) moiety became noticeable at 695 nm only at an increased concentration of 4.5×10^{-4} M in $CHCl_3$

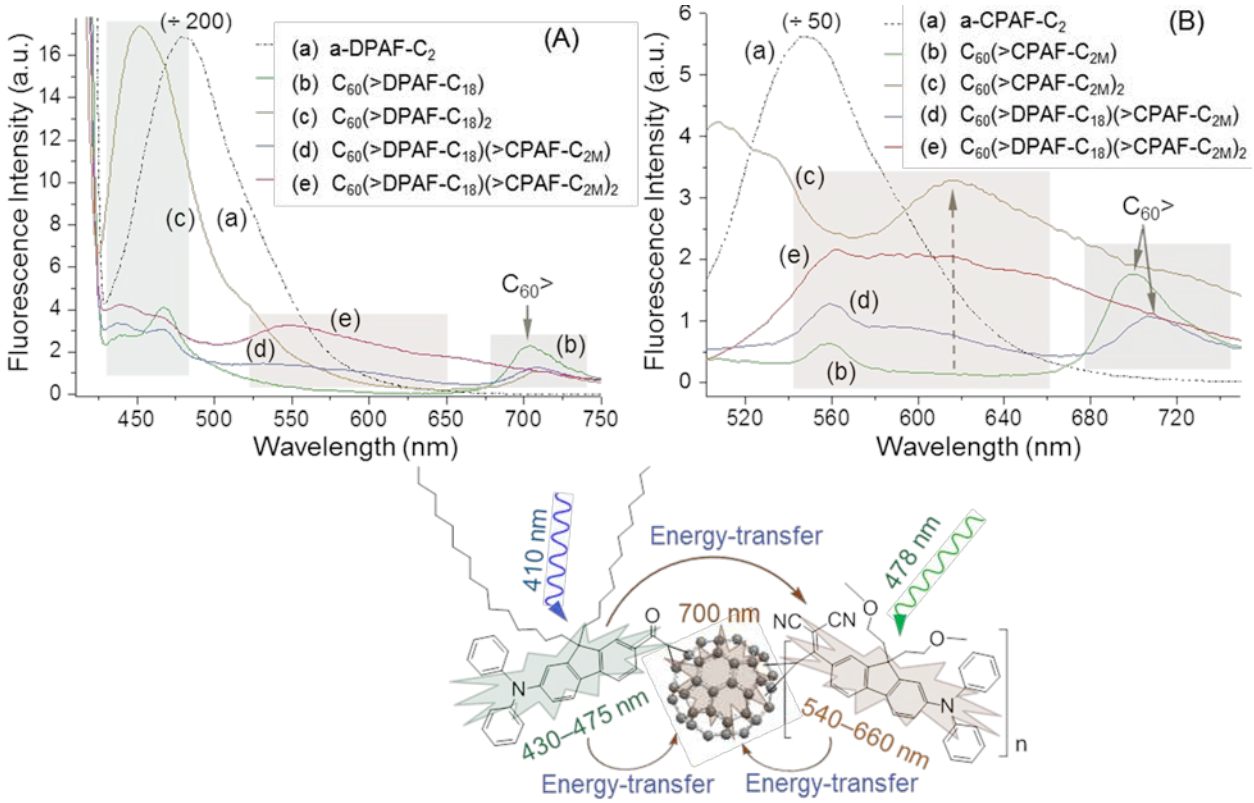

Figure 7. Steady-state fluorescence spectra of (A) (a) **10**, (b) **1** (including a Raman peak at 470 nm), (c) C_{60}(>DPAF-C_{18})$_2$, (d) **3**, and (e) **4** at the excitation wavelength of 410 nm and (B) (a) **11**, (b) **2** (including a Raman peak at 558 nm), (c) C_{60}(>CPAF-C_{2M})$_2$, (d) **3**, and (e) **4** at the excitation wavelength of 478 nm. The concentration of all samples was 1.0×10^{-5} M in toluene.

It is noteworthy that excited state intramolecular energy-transfer resonance phenomena between the DPAF-C_{18} and CPAF-C_{2M} antenna around the cage surface of **3** and **4** were observed. We first characterized the steady-state fluorescence (FL) emission of each antenna component using the model compound a-DPAF-C_2 **10** and a-CPAF-C_2 **11** (Scheme 1) in toluene as the spectroscopic reference. Upon photoexcitation of 10 at 410 nm to match with the optical absorption band of DPAF-C_{18}, strong fluorescence emissions of ^{1}(a-DPAF-C_2)* centered at 481 nm ($\lambda_{max,em}$) (Figure 7Aa) were detected. Likewise, strong FL emissions of ^{1}(a-CPAF-C_2)* centered at 543 nm ($\lambda_{max,em}$) (Figure 7Ba) were observed when 11 was irradiated at 478 nm which matches with the optical absorption band of CPAF-C_{2M}. As expected, highly efficient intramolecular fluorescence quenching of these two bands by C_{60} occurred when **1** and **2** were photoexcited at the same corresponding light wavelength, as shown in Figures 7Ab and 7Bb, respectively. This photophysical event led to the subsequent emission from the ^{1}(C_{60}>)* → ^{1}(C_{60}>)$_o$ transition at 704 and 708 nm, respectively. The possible phosphorescence emission from ^{3}(C_{60}>)* → ^{1}(C_{60}>)$_o$ transition expected at ~800–850 nm was too weak to be detected. In the case of the bisadduct C_{60}(>DPAF-C_{18})$_2$,[26] two FL bands with λ_{max} at 451 and 525 (shoulder) nm (Figure 7Ac) were shown, indicating incomplete quenching of C_{60}[>^{1}(DPAF)*-C_{18}]$_2$ by C_{60}> when the number of antenna are more than one. Similarly, three fluorescence bands with λ_{max} at 506, 531, and 615 (broad) nm (Figure 7Bc) were found for the bisadduct C_{60}(>CPAF-C_{2M})$_2$. Owing to high similarity on the

structural moieties, these FL bands were used as the reference for the FL spectroscopic characterization of **3** and **4**.

Interestingly, upon photoexcitation of the triad **3** specifically on the DPAF-C_{18} antenna moiety at 410 nm, the resulting FL spectrum (Figure 7Ad) displayed a weak broad FL band at 448 [from ^{1}(DPAF)*-C_{18}] and broad bands at 525–650 nm along with the ^{1}(C_{60}>)* emission band centered at 708 nm. The latter broad bands fit in the similar range as those of C_{60}[>^{1}(CPAF)*-C_{2M}]$_2$. As the number of CPAF-C_{2M} antenna being increased by one to the structure of tetrad C_{60}(>DPAF-C_{18})(>CPAF-C_{2M})$_2$ **4**, the intensity of broad FL bands at 525–650 nm became more pronounced while retaining the same intensity of the ^{1}(C_{60}>)* emission band at 709 nm (Figure 7Ae). The data revealed intramolecular Förster energy-transfer resonance from the photoexcited C_{60}[>^{1}(DPAF)*-C_{18}](>CPAF-C_{2M})$_2$ state to both $^1C_{60}$*(>DPAF-C_{18})(>CPAF-C_{2M})$_2$ and C_{60}(>DPAF-C_{18})[>^{1}(CPAF)*-C_{2M}]$_2$ states. The latter energy-transfer is possible since (i) the energy level of ^{1}(CPAF)*-C_{2M} is lower than that of ^{1}(DPAF)*-C_{18}, (ii) the energy of this FL band at 430–475 nm is slightly higher than that of the CPAF-C_{2M} absorption λ_{max} at 500 nm, and (iii) there is a partial overlap of emission/absorption bands to enhance the energy-transfer efficiency. Conversely, photoexcitation of 3 specifically on the CPAF-C_{2M} antenna moiety at 478 nm, the resulting FL spectrum (Figure 7Bd) showed only a weak broad FL band at 540–660 nm along with the ^{1}(C_{60}>)* emission band centered at 707 nm. Intensity of the former broad band was significantly increased using **4** (Figure 7Be) with photoexcitation on both two CPAF-C_{2M} antenna moieties. This confirmed the band was contributed from the C_{60}(>DPAF-C_{18})[>^{1}(CPAF)*-C_{2M}]$_2$ state, which was capable of inducing the $^1C_{60}$*(>DPAF-C_{18})(>CPAF-C_{2M})$_2$ state subsequently.

4.2. Time-Resolved Emission and Transient Absorption Measurements

Intramolecular energy- or electron-transfer related photophysical events from photoexcited DPAF-C_{18}/CPAF-C_{2M} antenna moiety to the C_{60} cage of **3** and **4** occurred in a competitive process with the energy-transfer process being more favorable in less polar solvents, such as toluene.[34] Both events were responsible for the significant reduction in intensity of ^{1}(DPAF)*-C_{18} or ^{1}(CPAF)*-C_{2M} derived emission. In the case of C_{60}(>CPAF-C_n), possible electron-transfer processes from either partially polarized C_{60}[>(DCE)$^{-\delta}$-(DPAF)$^{+\delta}$-C_2] or C_{60}[>^{1}(CPAF)*-C_2] states in *o*-DCB and PhCN to the corresponding C_{60}^{-}·(>CPAF^{+}·-C_2) state were considered as possible quenching pathways in addition to the alternative energy-transfer process from C_{60}[>^{1}(CPAF)*-C_2] to the C_{60}> moiety yielding $^1C_{60}$*(>CPAF-C_2) in toluene.[33] In this study, we carried out time-correlated single photon counting experiments for **3** and **4** to follow its emission decay lifetimes in ns region using a 70-ps diode laser operated at the excitation energy of 375 nm in air-saturated toluene, as shown in Figure 8. The emission profile was monitored at the 448-nm peak corresponding to that of the photoexcited C_{60}[>^{1}(DPAF)*-C_{18}](>CPAF-C_{2M})$_{1or2}$ state. The detailed data including lifetimes were summarized in Table 1.

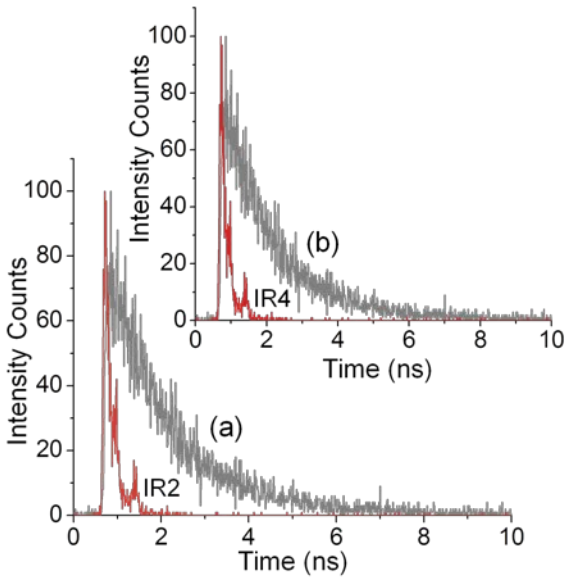

Figure 8. Time-correlated emission decay of (a) C_{60}(>DPAF-C_{18})(>CPAF-C_{2M}) **3** and (b) C_{60}(>DPAF-C_{18})(>CPAF-C_{2M})$_2$ **4** at 448 nm (λ_{max} of the DPAF-C_{18} fluorescence band) in air saturated toluene following excitation at 375 nm using a 70-ps diode laser. Lifetimes were given in Table 1.

In both cases of **3** and **4**, we observed a biexponential decay profile of the emission with the bulk of decay belonging to the longer lifetimes. The emission profile from the $^1C_{60}$*(>DPAF-C_{18})(>CPAF-C_{2M})$_{1or2}$ state at the 718-nm peak was not possible to follow for calculation of its lifetime due to a very weak signal. As a result, the fast growth and long-lived emission lifetimes (τ_s) of

^{1}(DPAF)*-C_{18} moiety of **3** were calculated to be 80 and 1286 ps, respectively. The same measurements on the compound **4** gave two τ_s values of 91 and 1068 ps with a slightly longer lifetime for the fast growth decay. By using the emission decay rate data of the monoadduct C_{60}[>^{1}(DPAF)*-C_9] for comparison, its two τ_s values of <50 [within the instrument response function (IRF) limit of 50 ps] and 1402 ps, monitored at the 454-nm peak, indicated a much shorter lifetime for the fast growth emission decay than that of **3** and **4**. The extremely short decay lifetime revealed ultrafast intramolecular energy-transfer kinetics of the donor (D) ^{1}(DPAF)*-C_9 antenna of C_{60}(>DPAF-C_9) to the C_{60} acceptor (A) cage moiety resulting in the formation of $^1C_{60}$*(>DPAF-C_9) that was estimated to be 130 fs by femtosecond pump-probe transient absorption spectroscopy measurement.[15] The occurrence of this photophysical phenomena was explained by the molecular structure design since the periconjugation bonding linked D–A components within a separation distance of only 2.6–3.5 Å, as determined by x-ray single crystal structural analysis of C_{60}(>DPAF-C_2) and C_{60}(>CPAF-C_2).[15,32] Accordingly, the observation of a longer decay lifetime of 80–90 ps for **3**/**4** implied a second energy-transfer mechanism that occurred at a slower rate between chromophores due to a longer through-space distance. This argument is reasonable since the functional covalent linker between C_{60} and the antenna component is identical among all these compounds for the same ultrafast photophysical processes through the D–A bond. The steady-state fluorescence spectra of **3** and **4** displayed the FL emission of C_{60}(>DPAF-C_{18})[>^{1}(CPAF)*-C_{2M}]$_{1or2}$ at 525–650 nm upon the excitation of the DPAF-C_{18} antenna moiety at 410 nm. The phenomenon was interpreted as the intramolecular energy-transfer from the photoexcited ^{1}(DPAF)*-C_{18} moiety to the CPAF-C_{2M} antenna moiety around the C_{60} cage surface. The time-resolved emission data fitted well with this conclusion that was also consistent with data that both IR and ^{1}H NMR spectroscopic analyses of **3** and **4**, indicated 2–3 regioisomers having the average separation distance among DPAF-C_{18} and CPAF-C_{2M} antenna in greater than 90^o (or >5.0 Å) at the surface of cage sphere. With multiple antenna attachments on a C_{60} each distributing from the north-pole area to either the equator or south-pole regions, we should observe efficient Förster energy-transfer resonance events going from a high-energy antenna unit, such as DPAF-C_{18}, to low-energy antenna units, such as CPAF-C_{2M}, in a cascade fashion.

Table 1. Photophysical properties of the hybrid triad **3**, tetrad **4**, and related model compounds in air saturated toluene[a]

Compound	λ_{max} (abs.)	ε (M^{-1} cm^{-1})	λ_{max} (FL)	τ_s [^{1}(C_{60}>)* or ^{1}(DPAF)*]	λ_{max} (T_1–T_n, abs.)	τ_t^f [^{3}(C_{60}>)*]
C_{60}	335 nm	51800	--	--	750 nm	3.7 μs
C_{60}>	332 nm	48600	708 nm	1350 ps (at 708 nm)	720 nm	24 μs
C_{60}(>DPAF-C_9)	404 nm	39200	454 nm; 700 nm[b]	<50 ps; 1402 ps (at 454 nm)	720 nm[c]	40 μs[c]
C_{60}(>CPAF-C_{12})	485 nm	18900	608 nm; 703 nm	--	720 nm	44 μs
3	413 nm 494 nm	39000 23000	448 nm[d] 525–650 nm[d] 708 nm[d]	80 ps; 1286 ps (at 448 nm)	705 nm	31 μs
4	417 nm 500 nm	46000 46000	448 nm[d] 540–660 nm[e] 707 nm[e]	91 ps; 1068 ps (at 448 nm)	690 nm	29 μs

[a] It included the lifetimes τ_s of transient C_{60}[>^{1}(DPAF)*-C_{18}](>CPAF-C_{2M})$_{1or2}$ state and τ_t of transient $^3C_{60}$*(>DPAF-C_{18})(>CPAF-C_{2M})$_{1or2}$ state, where the data based on DPAF-C_n, CPAF-C_n, and C_{60}> moieties were marked by green, brown, and black, respectively. [b] Data measured in hexane. [c] Data measured in benzene. [d] Excitation at 410 nm. [e] Excitation at 478 nm. [f] Samples deoxygenated via freeze pump thaw.

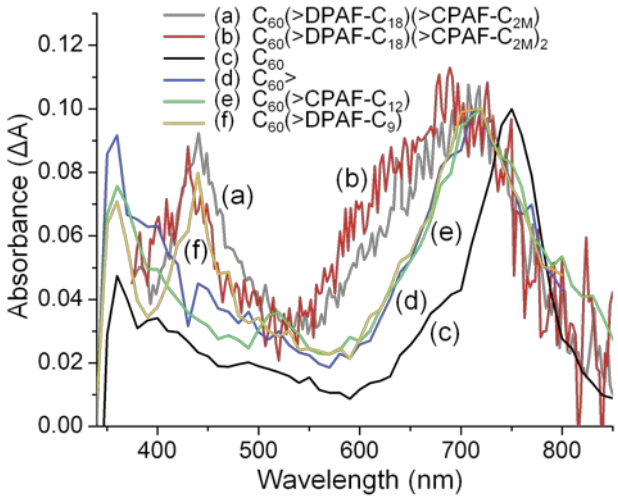

Figure 9. Transient absorption spectra of (a) C_{60}(>DPAF-C_{18})(>CPAF-C_{2M}) **3** and (b) C_{60}(>DPAF-C_{18})(>CPAF-C_{2M})$_2$ **4** upon photoexcitation at 355 nm in deoxygenated toluene with a 5-ns pulse laser, in comparison with those of C_{60}, C_{60}>, C_{60}(>CPAF-C_{12}), and C_{60}(>DPAF-C_9).

We also carried out nanosecond laser flash photolysis experiments to measure the triplet excited state properties of the hybrid triad **3** and tetrad **4**. In the measurement, the samples were excited at 355 nm with a 5.0-ns pulse laser (Q-switched Nd:YAG) in deoxygenated toluene followed by probing using the white light. Resulting transient absorption spectra as normalized for the comparison with those of C_{60}, C_{60}>, C_{60}(>CPAF-C_{12}), and C_{60}(>DPAF-C_9) were shown in Figure 9. The ns transient absorption profile of methano[60]fullerene (C_{60}>, Figure 9d) displayed a clear shift of the T_1–T_n absorption band of ^{3}(C_{60}>)* to 720 nm from that of the pristine $^3C_{60}$* at 750 nm (Figure 9c). This band was in nearly identical wavelengths for both $^3C_{60}$*(>CPAF-C_{12}) (Figure 9e) and $^3C_{60}$*(>DPAF-C_9) (Figure 9f) that can be used as the reference band for the characterization of **3** and **4**. The excitation wavelength of 355 nm was chosen for specifically the activation of DPAF-C_{18} antenna moiety of **3** and **4**. Therefore, we expected to detect the transient absorption band of C_{60}[>^{1}(DPAF)*-C_{18}](>CPAF-C_{2M})$_{1or2}$ at 430–440 nm (Figures 9a and 9b), in a nearly identical range to that of C_{60}[>^{1}(DPAF)*-C_9] (Figure 9f). In the recent report on the photophysical property characterization of C_{60}(>DPAF-C_9),[15] the intersystem energy crossover from the $^1C_{60}$*(>DPAF-C_9) state to its triplet $^3C_{60}$*(>DPAF-C_9) state was found to occur in ~1.4 ns with triplet excited state lifetime of 40 μs in benzene (Table 1). Thus, by the use of a 5.0-ns pulse in the current experiment, There should be sufficient time for the excitation and formation of $^3C_{60}$*(>DPAF-C_{18})(>CPAF-C_{2M})$_{1or2}$. Detection of the 430–440 nm band may imply incomplete energy-transfer from the ^{1}(DPAF)*-C_{18} moiety to C_{60}> as compared with nearly complete energy-transfer from the ^{1}(CPAF)*-C_{2M} moiety to C_{60}> since no significant transient absorption of C_{60}[>^{1}(CPAF)*-C_{12}] (Figure 4e) was found. Furthermore, observation of a new broad band at 550–650 nm in Figures 9a and 9b corresponding to the ns transient absorption of C_{60}(>DPAF-C_{18})[>^{1}(CPAF)*-C_{2M}]$_{1or2}$ may also be indicative of a slower rate of Förster resonance energy-transfer from the ^{1}(DPAF)*-C_{18} antenna to CPAF-C_{2M} antenna occurring in the sub-ns to ns region, consistent with the measured long-lived emission decay lifetimes of C_{60}[>^{1}(DPAF)*-C_{18}](>CPAF-C_{2M})$_{1or2}$ in the similar time scale (Figure 8).

4.3. Two-Photon Absorption (2PA) by Both *Z*-Scans and Light-Intensity-Dependent Transmittance Measurements

Simultaneous 2PA cross-sections (σ_2) and nonlinear light-transmittance measurements of **3** and **4** were carried out in toluene at wavelengths of either 780 or 980–1000 nm with the collection of femtosecond *Z*-scan data to demonstrate the nonlinear photoresponse ability of hybrid C_{60}-(antenna)$_{2–3}$ analogous triads and tetrads at different near-IR wavelength ranges. A C_{60}-(antenna)$_x$ nanostructure showing large 2PA-active NLO properties at many wavelengths or a continuous wavelength spectrum will facilitate their uses as broadband NLO materials. In the molecular structure of **3** and **4**, all chromophore components are 2PA-responsive that allows the corresponding branched C_{60}-(antenna)$_x$ (x = 2–3) nanomaterials to exhibit appreciable 2PA cross-sections at three adjacent spectral ranges of 600–750 (based on C_{60}> moiety), 740–900 (based on DPAF-C_{18} moiety), and 860–1100 (based on CPAF-C_{2M} moiety) nm. These three ranges correspond to the strong linear optical absorption band of the C_{60}> cage at 280–375 nm, the DPAF-C_{18} antenna at 370–450 nm, and the CPAF-C_{2M} antenna at 430–550 nm.

By tuning the ratio of CPAF-C_{2M}/DPAF-C_{18} to two, a nearly even linear absorption extinction coefficient over 400–520 nm was achieved for creating the corresponding broadband 2PA features over 800–1050 nm with no apparent absorption minimum.

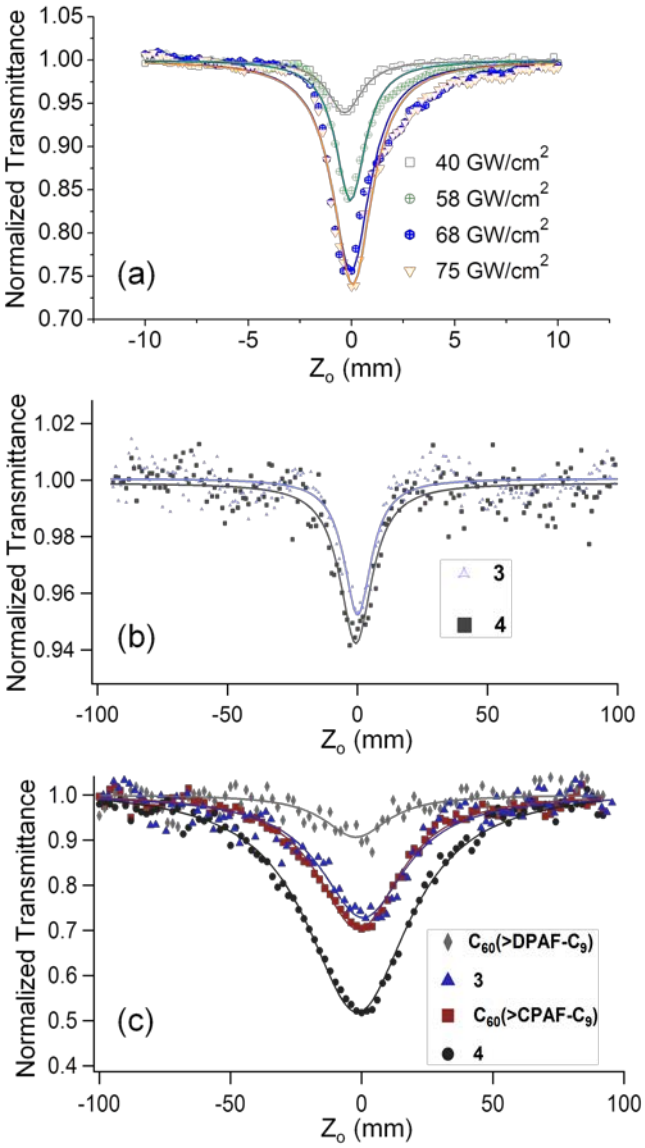

Figure 10. Open-aperture *Z*-scan profiles of (a) C_{60}(>DPAF-C_9)(>CPAF-C_{2M}) using laser pulses working at 780 nm with a 150-fs duration ([*C*] = 1.6 × 10^{-3} M in toluene), (b) C_{60}(>DPAF-C_{18})(>CPAF-C_{2M}) **3** and C_{60}(>DPAF-C_{18})(>CPAF-C_{2M})$_2$ **4** using 125 fs laser pulses operated at 800 nm and the input intensity of 270 GW/cm^2, and (c) fullerene derivatives C_{60}(>DPAF-C_9), C_{60}(>CPAF-C_9), **3**, and **4** using 125-fs laser pulses operated at 980 nm and the input intensity of 104 GW/cm^2. Measurements of (b) and (c) were carried out at the concentration of 5 × 10^{-3} M in toluene.

The use of fs pulses eliminates potential accumulative thermal scattering effects in the material environment. A pulse duration width of 125 fs was used to focus the study primarily on the 2PA process of each antenna. This pulse width matches with the value of 130 fs required for the effective intramolecular energy-transfer from the excited antenna to the C_{60}> moiety, as discussed above. Therefore, the measured σ_2 values at 125 fs should not cover the excited singlet state absorption (S_1–S_n) of $^1C_{60}$*(>DPAF-C_{18})(>CPAF-C_{2M})$_{1or2}$ cage moiety. As a result, open-aperture *Z*-scan data of two hybrid triads C_{60}(>DPAF-C_9)(>CPAF-C_{2M}) and C_{60}(>DPAF-C_{18})(>CPAF-C_{2M}) **3** and one hybrid tetrad C_{60}(>DPAF-C_{18})(>CPAF-C_{2M})$_2$ **4** at 780–800 and 980 nm in toluene under different conditions were shown in Figure 10 with all parameters summarized in Table 2. For the comparison and discussion purpose, the σ_2 values of C_{60}(>CPAF-C_9) and C_{60}(>DPAF-C_9) were also included. The method for data reduction, line fitting, and 2PA cross-section calculation was described in the experimental section.

We used the sample of C_{60}(>CPAF-C_9) to demonstrate the strong concentration-dependent σ_2 values through solution concentration between 10^{-3}–10^{-2} M (Table 2) owing to the aggregation effect. Only a moderate σ_2 value of 46 GM was measured at the concentration of 1.0 × 10^{-2} M. A 5–6 folds increase of the σ_2 value to 275 GM was achieved by simply decreasing the concentration to 1.0 × 10^{-3} M. The phenomena were much more pronounced for the dyad C_{60}(>DPAF-C_9) when the irradiation wavelength of 780 nm matched with two-photon absorption of DPAF-C_9 antenna. In this case, a 70-fold increase in the σ_2 value to 2190 GM was measured at 1.0 × 10^{-4} M, as compared with a 30 GM value at 1.0 × 10^{-2} M.[31] Since the 2PA measurement was performed at the focal area of the laser pulse, the signal intensity could be as low at 10^{-4} M leading to less accuracy in the calculation and line-fitting of the Z-scan data. Therefore, we used a medium concentration of 2.0–5.0 × 10^{-3} M for this study.

Table 2. Two-photon absorption cross-sections (σ_2) of dyads C_{60}(>DPAF-C_9) and C_{60}(>CPAF-C_9), hybrid triads **3** and **3**-C_9, and the hybrid tetrad **4** at 780 nm[a]

Compound	[C] /M	I /GW cm^{-2}	β /cm GW^{-1}	σ_2 /10^{-48} cm^4 s photon^{-1} molecule^{-1}
C_{60}(>DPAF-C_9)[b]	1.0×10^{-4}	163	0.036	21.9 (2190 GM)[c]
	1.9×10^{-3}	163	0.080	8.0 (800 GM)[c]
	1.0×10^{-2}	163	0.100	0.3 (30 GM)[c]
C_{60}(>CPAF-C_9)[d]	1.0×10^{-3}	220	0.0065	2.75 (275 GM)
	2.0×10^{-3}	220	0.0080	1.69 (169 GM)
	1.0×10^{-2}	220	0.0110	0.46 (46 GM)
3-C_9[e]	1.6×10^{-3}	40	0.035	1.30 (130 GM)
3	5.0×10^{-3}	270	0.034	2.21 (221 GM)
4	5.0×10^{-3}	270	0.04	2.66 (266 GM)

[a] Measured using laser pulses working with a 125-fs duration and a repetition rate of 1.0 kHz, or with different conditions indicated. [b] Measured in CS_2 with 150-fs laser pulses at 800 nm.[31] [c] Corrected value by deduction of the β value of CS_2 as the background correction. [d] Measured in THF with 226-fs laser pulses. [e] The triad C_{60}(>DPAF-C_9)(>CPAF-C_{2M}) measured in toluene with 150-fs laser pulses at 800 nm.

It is interesting to note that, even though the irradiation wavelength of 780 nm was not the best fit to the 2PA absorption λ_{max} of C_{60}(>CPAF-C_9) at 1000 nm, we still observed appreciable cross-section values. This could be owing to C_{60}-(antenna)$_x$ nanostructures in general acting as broadband NLO materials since the optical absorption of the chromophore component covers a broad wavelength range. In the comparison between hybrid triads **3**, C_{60}(>DPAF-C_{18})(>CPAF-C_{2M}), and **3**-C_9, C_{60}(>DPAF-C_9)(>CPAF-C_{2M}), we noticed that the use of long *n*-octadecyl chains (C_{18}) in **3** increased the solubility of nanostructure in toluene, as compared with that of the branched 3,5,5-trimethylhexyl (C_9) groups in **3**-C_9, and was able to produce a slightly higher 2PA σ_2 value of 221 GM, even though the measurement was made by a solution with 3 times higher in concentration. This value is much lower than that of C_{60}(>DPAF-C_9) in CS_2. Apparently, the solvent effect arising from CS_2 may play a significant role in the value of σ_2. For the hybrid tetrad **4**, the σ_2 value of 266 GM was slightly higher than that of **3** since the number of photoresponsive DPAF-C_{18} antenna was the same for both structures. An additional CPAF-C_{2M} antenna in **4** increased its $\sigma_2$value by 45 GM.

The second set of *Z*-scan experiments were performed in toluene using a pulse laser with a 125-fs pulse duration width at 980 nm to match with the linear absorption λ_{max} of the CPAF-C_{2M} antenna at 500 nm. As expected, the 2PA cross-section values of C_{60}(>DPAF-C_9) as 85 (I = 48) and 130 (I = 104 GM/cm^2) GM (Table 3) were found to be moderate at the concentration of 5.0×10^{-3} M since the 2PA energy at 980 nm is less than the main linear absorption λ_{max} (408 nm) of the DPAF-C_9 antenna. Higher 2PA σ_2 values of 450 (I = 48) and 538 (I = 104 GM/cm^2) GM for C_{60}(>CPAF-C_9) were measured in similar experiments, consistent with using well-matched absorption and excitation wavelengths. With an additional DPAF-C_{18} arm attached to the structure of **3**, no increase of σ_2 values was found with σ_2 = 504 GM (I = 104 GM/cm^2) in the same range as that of C_{60}(>CPAF-C_9). As the number of 980-nm-responsive antenna was increased to two in the structure of hybrid tetrad **4**, C_{60}(>DPAF-C_{18})(>CPAF-C_{2M})$_2$, the σ_2 values were doubled to 995 (I = 48) and 1100 (I = 104 GM/cm^2) GM. These data further demonstrated the suitability of **3** and **4** to be used as broadband NLO materials at 780–1000 nm.

Table 3. Two-photon absorption cross-sections (σ_2) of hybrid dyads C_{60}(>DPAF-C_9) and C_{60}(>CPAF-C_9), the hybrid triad **3**, and the hybrid tetrad **4** at 980 nm in toluene[a]

Compound	[C] /M	I /GW cm^{-2}	β /cm GW^{-1}	σ_2 /10^{-48} cm^4 s photon^{-1} molecule^{-1}
C_{60}(>DPAF-C_9)	5.0×10^{-3}	104	0.0198	1.3 (130 GM)
		48	0.0129	0.85 (85 GM)
C_{60}(>CPAF-C_9)	5.0×10^{-3}	104	0.0815	5.38 (538 GM)
		48	0.0677	4.5 (450 GM)
3	5.0×10^{-3}	104	0.0765	5.04 (504 GM)
		48	0.0468	3.1 (310 GM)
4	5.0×10^{-3}	104	0.166	11 (1100 GM)
		48	0.144	9.5 (950 GM)

[a] Measured using laser pulses working with a 125-fs pulse duration and the light intensity I indicated.

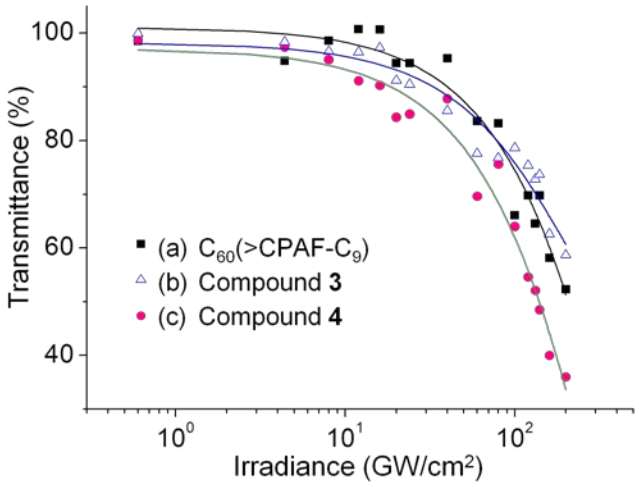

Figure 11. Nonlinear transmittance of (a) C_{60}(>CPAF-C_9), (b) C_{60}(>DPAF-C_{18})(>CPAF-C_{2M}), and (c) C_{60}(>DPAF-C_{18})(>CPAF-C_{2M})$_2$ as a function of light intensity. All measurements were carried out with 125-fs laser pulses operated at 980 nm and the concentration of 5×10^{-3} M in toluene.

Nonlinear light-transmittance measurements of C_{60}(>CPAF-C_9), **3**, and **4** were performed as a function of irradiance intensity with 125-fs laser pulses at 980 nm with the concentration of 5×10^{-3} M in toluene. As shown in Figure 10c, the *Z*-scans displayed positive signs for absorption nonlinearities with a decreasing trend of light-transmittance in the order of **4** > **3** ≈ C_{60}(>CPAF-C_9) > C_{60}(>DPAF-C_9) in solution with the input intensity of 104 GW/cm^2. Accordingly, the plot of transmittance (%) vs irradiance (GW/cm^2) of all samples showed a linear transmission (T = ~95%) with input intensity of up to 20 GW/cm^2. When the incident light intensity was increased above 30 GW/cm^2, the transmittance (%) began to deviate from the linear transmission line and decrease indicating the initiation of nonlinearity and the transmittance reduction effect. The transmitted fluence further departed from the linear line upon the increase in the incident fluence. A trend showing higher efficiency in reducing light-transmittance down to 50, 55, and 35% for C_{60}(>CPAF-C_9), **3**, and **4**, respectively, was observed with the increase of light intensity up to 110 GW/cm^2 (Figure 11). The observed improvement in lowering the transmitted light-intensity by **4** is consistent with its better nonlinear contribution that can be correlated to its higher fs 2PA cross-sections, as shown by the *Z*-scans.

5.0 CONCLUSION

We demonstrated the design, synthesis, structural characterization, and study of photophysical properties of ultrafast photoresponsive starburst and dendritic C_{60}/C_{70}-light harvesting antenna-based

organic nanostructures for broadband nonlinear optical (NLO) nanomaterial applications. Specifically, we provided evidence by, as example, two C_{60}-(antenna)$_x$ analogous compounds as the branched hybrid triad C_{60}(>DPAF-C_{18})(>CPAF-C_{2M}) **3** and tetrad C_{60}(>DPAF-C_{18})(>CPAF-C_{2M})$_2$ **4** nanostructures. Multiple light-harvesting donor antenna chromophores were bound on a C_{60} acceptor by periconjugation within 2.6–3.5 Å of the physical separation distance. The structural design was intended to facilitate the ultrafast femtosecond intramolecular energy-transfer process from the photoexcited C_{60}[$>^1$(DPAF)*-C_{18}](>CPAF-C_{2M})$_{1or2}$ or C_{60}(>DPAF-C_{18})[$>^1$(CPAF)*-C_{2M}]$_{1or2}$ to the C_{60}> cage moiety upon two-photon pumping at either 780 or 980 nm, respectively. The nanostructure of hybrid tetrad **4** showed nearly equal absorption in extinction coefficients over the wavelength range of 400–550 nm that corresponds to near-IR two-photon based excitation wavelengths at 780–1100 nm for broadband NLO applications. Aside from their enhanced 2PA activity at 780 nm, we demonstrated, for the first time, the ability of C_{60}-(antenna)$_x$ analogous nanostructures to exhibit ultrafast photo-responses at 980 nm showing 2PA cross-section (σ_2) values of 995–1100 GM for the tetrad. These σ_2 values were correlated to the observed good efficiency in reducing fs light-transmittance down to 35% at the light intensity of 110 GW/cm^2. Accordingly, 2PA characteristics of these nanostructures at multiple NIR wavelengths provided support for their suitability in uses as broadband NLO nanomaterials at 600–1100 nm that includes the 2PA ability of two antenna, DPAF (700–850 nm) and CPAF (850–1100 nm), and the fullerene cage at shorter wavelengths (600–700 nm). We also found that the unique feature of intramolecular Förster energy-transfer phenomena from the photoexcited high-energy DPAF-C_{18} antenna unit to the low-energy CPAF-C_{2M} moiety at the fullerene cage surface gave the fluorescence emission at slightly longer wavelengths than 600 nm in a cascade fashion. It may be correlated to and provide an interesting mechanism for the enhancement of 2PA cross-section values of these hybrid C_{60}-(antenna)$_x$ nanostructures.

6.0 REFERENCES

(1) Tutt, L. W.; Boggess, T. F. A Review of Optical Limiting Mechanisms and Devices Using Organics, Fullerenes, Semiconductors and Other Materials. *Progr. Quant. Electr.* **1993**, *17*, 299–338.

(2) Sun, Y.-P.; Riggs, J. E. Organic and Inorganic Optical Limiting Materials. From Fullerenes to Nanoparticles. *Int. Rev. Phys. Chem.* **1999**, *18*, 43–90.

(3) McGeoch, S. P.; Thomson, I.; Christie, A.; Hollins, R. C. Design Considerations for Using Optical Limiters in Sighting Systems. *Nonlinear Optics* **1999**, *21*, 491–502.

(4) Bhawalkar, J. D.; Kumar, N. D.; Zhao, C.-F.; Prasad, P. N. Two-Photon Photodynamic Therapy. *J. Clin. Laser Med. Surge.* **2009**, *15*, 201−204.

(5) Brown, S. Photodynamic Therapy: Two Photons are Better than One. *Nat. Photonics* **2008**, *2*, 394−395.

(6) Spangler, C. W.; Starkey, J. R.; Dubinina, G.; Fahlstrom, C.; Shepard, J. Optimization of Targeted Two-Photon PDT Triads for the Treatment of Head and Neck Cancers. *Proc. SPIE* **2012**, *8207*, 820720.

(7) Spangler, C. W.; Rebane, A.; Starkey, J.; Drobizhev, M. Targeted Two-Photon PDT Photo-sensitizers for the Treatment of Subcutaneous Tumors. *Proc. SPIE* **2009**, *7380*, 73803.

(8) Dahlstedt, E.; Collins, H. A.; Balaz, M.; Kuimova, M. K.; Khurana, M.; Wilson, B. C.; Phillips, D.; Anderson, H. L. One- and Two-Photon Activated Phototoxicity of Conjugated Porphyrin Dimers with High Two-Photon Absorption Cross Sections. *Org. Biomol. Chem.* **2009**, *7*, 897–904.

(9) Riggs, J. E.; Sun, Y.-P. Optical Limiting Properties of [60]Fullerene and Methano[60]fullerene in Solution versus in Polymer Matrix: the Role of Bimolecular Processes and a Consistent Nonlinear Absorption Mechanism. *J. Phys. Chem. A* **1999**, *103*, 485–495.

(10) Maggini, M.; De Faveri, C.; Scorrano, G.; Prato, M.; Brusatin, G.; Guglielmi, M.; Meneghetti, M.; Signorini, R.; Bozio, R. Synthesis and Optical-Limiting Behavior of Hybrid Inorganic–Organic Materials from the Sol–Gel Processing of Organofullerenes. *Chem. Eur. J.* **1999**, *5*, 2501–2510.

(11) Chiang, L. Y.; Padmawar, P. A.; Canteenwala, T.; Tan, L.-S.; He, G. S.; Kannan, R.; Vaia, R.; Lin, T.-C.; Zheng, Q.; Prasad, P. N. Synthesis of C_{60}-Diphenylaminofluorene Dyad with Large 2PA Cross-Sections and Efficient Intramolecular Two-Photon Energy Transfer. *Chem. Commun.* **2002**, 1854–1855.

(12) Koudoumas, E.; Konstantaki, M.; Mavromanolakis, A.; Couris, S.; Fanti, M.; Zerbetto, F.; Kordatos, K.; Prato, M. Large Enhancement of the Nonlinear Optical Response of Reduced Fullerene Derivatives. *Chem. Eur. J.* **2003**, *9*, 1529–1534.

(13) Padmawar, P. A.; Canteenwala, T.; Verma, S.; Tan, L.-S.; Chiang, L. Y. Synthesis and Photophysical Properties of C_{60}-Diphenylaminofluorene Dyad and Multiads. *J. Macromol. Sci., Part A: Pure Appl. Chem.* **2004**, *41*, 1387–1400.

(14) Padmawar, P. A.; Canteenwala, T.; Verma, S.; Tan, L.-S.; Chiang, L. Y. Synthesis and Characaterization of Two-Photon Absorbing Diphenylaminofluorenocarbonyl-methano[60]fullerenes. *J. Mater. Chem.* **2006**, *16*, 1366–1378.

(15) Padmawar, P. A.; Rogers, J. E.; He, G. S.; Chiang, L. Y.; Tan, L.-S.; Canteenwala, T.; Zheng, Q.; Slagle, J. E.; McLean, D. G.; Fleitz, P. A. et al. Large Cross-Section Enhancement and Intramolecular Energy Transfer upon Multiphoton Absorption of Hindered Diphenylaminofluorene-C_{60} Dyads and Triads. *Chem. Mater.* **2006**, *18*, 4065–4074.

(16) Kopitkovas, G.; Chugreev, A.; Nierengarten, J. F.; Rio, Y.; Rehspringer, J. L.; Hönerlage, B. Reverse Saturable Absorption of Fullerodendrimers in Porous SiO_2 Sol-Gel Matrices. *Opt. Mater.* **2004**, *27*, 285–291.

(17) He, G. S.; Tan, L.-S.; Zheng, Q.; Prasad, P. N. Multiphoton Absorbing Materials: Molecular Designs, Characterizations, and Applications. *Chem. Rev.* **2008**, *108*, 1245−1330.

(18) Spangler, C. Recent Development in the Design of Organic Materials for Optical Power Limiting. *J. Mater. Chem.* **1999**, *9*, 2013–2020.

(19) McKay, T. J.; Staromlynska, J.; Wilson, P.; Davy, J. Nonlinear Luminescence in a Pt:ethynyl Compound. *J. Appl. Phys.* **1999**, *85*, 1337–1341.

(20) Perry, J. W. Organic and Metal-Containing Reverse Saturable Absorbers for Optical Limiters. In *Nonlinear Optics of Organic Molecules and Polymers*, Nalwa, H. S.; Miyata, S., Eds. CRC Press: Boca Raton, 1997; pp. 813–840.

(21) Henari, F. Z.; Cazzini, K. H.; Weldon, D. N.; Blau, W. J. All Optical Switching Based on Intensity Induced Absorption in C_{60}. *Appl. Phys. Lett.* **1996**, *68*, 619–621.

(22) Elim, H. I.; Ouyang, J.; Goh, S. H.; Ji, W. Optical-Limiting-Based Materials of Mono-functional, Multifunctional and Supramolecular C_{60}-Containing Polymers. *Thin Solid Films* **2005**, *477*, 63–72.

(23) Rodenberger, D. C.; Heflin, J. R.; Garito, A. F. Excited-State Enhancement of Optical Nonlinearities in Linear Conjugated Molecules. *Nature* **1992**, *359*, 309–311.

(24) Tutt, L. W.; Kost, A. Optical Limiting Performance of C_{60} and C_{70} Solutions. *Nature* **1992**, *356*, 225–226.

(25) Kost, A.; Tutt, L.; Klein, M. B.; Dougherty, T. K.; Elias, W. E. Optical Limiting with C_{60} in Poly(methyl methacrylate). *Opt. Lett.* **1993**, *18*, 334–336.

(26) He, G. S.; Xu, G. C.; Prasad, P. N.; Reinhardt, B. A.; Bhatt, J. C.; Dillard, A. G. Two-Photon Absorption and Optical-Limiting Properties of Novel Organic Compounds. *Opt. Lett.* **1995**, *20*, 435–437.

(27) For a review: Walter, M. G.; Rudine, A. B.; Wamser, C. C. Porphyrins and Phthalocyanines in Solar Photovoltaic Cells. *J. Porphyr. Phthalocyan.* **2010**, *14*, 759–792.

(28) Bottari, G.; de la Torre, G.; Guldi, D. M.; Torres, T. Covalent and Noncovalent Phthalocyanine−Carbon Nanostructure Systems: Synthesis, Photoinduced Electron Transfer, and Application to Molecular Photovoltaics. *Chem. Rev*. **2010**, *110*, 6768–6816.

(29) Schuster, D. I.; Cheng, P.; Jarowski, P. D.; Guldi, D. M.; Luo, C.; Echegoyen, L.; Pyo, S.; Holzwarth, A. R.; Braslavsky, S. E.; Williams, R. M. et al. Design, Synthesis, and Photophysical Studies of a Porphyrin-Fullerene Dyad with Parachute Topology; Charge Recombination in the Marcus Inverted Region. *J. Am. Chem. Soc*. **2004**, *126*, 7257–7270.

(30) Imahori, H.; Fukuzumi, S. Porphyrin- and Fullerene-Based Molecular Photovoltaic Devices. *Adv. Funct. Mater*. **2004**, *14*, 525–536.

(31) Elim, H. I.; Anandakathir, R.; Jakubiak, R.; Chiang, L. Y.; Ji, W.; Tan, L.-S. Large Concentration-Dependent Nonlinear Optical Responses of Starburst Diphenylaminofluorenocarbonyl methano[60]fullerene Pentaads. *J. Mater. Chem.* **2007**, *17*, 1826–1838.

(32) Chiang, L. Y.; Padmawar, P. A.; Rogers-Haley, J. E.; So, G.; Canteenwala, T.; Thota, S.; Tan, L.-S.; Pritzker, K.; Huang, Y.-Y.; Sharma, S. K. et al. Synthesis and Characterization of Highly Photoresponsive Fullerenyl Dyads with a Close Chromophore Antenna–C_{60} Contact and Effective Photodynamic Potential. *J. Mater. Chem.* **2010**, *20*, 5280–5293.

(33) El-Khouly, M. E.; Padmawar, P.; Araki, Y.; Verma, S.; Chiang, L. Y.; Ito, O. Photoinduced Processes in a Tricomponent Molecule Consisting of Diphenylaminofluorene-dicyanoethylene-methano[60]fullerene. *J. Phys. Chem. A* **2006**, *110*, 884–891.

(34) Luo, H.; Fujitsuka, M.; Araki, Y.; Ito, O.; Padmawar, P.; Chiang, L. Y. Inter- and Intramolecular Photoinduced Electron-Transfer Processes Between C_{60} and Diphenylaminofluorene in Solutions. *J. Phys. Chem. B* **2003**, *107*, 9312−9318.

(35) Feneyrou, P. Broadband Optical Limiting Using Tandem Filters with Multiphoton Absorber and Reverse Saturable Absorbers. *J. Nonlinear Opt. Phys. Mater*. **2000**, *9*, 523–530.

(36) Guldi, D.M.; Prato, M. Excited-state properties of C_{60} fullerene derivatives. *Acc. Chem. Res*. **2000**, *33*, 695−703.

(37) Fujitsuka, M.; Ito, O. Encyclopedia of Nanoscience and Nanotechnology, Ed. Nalwa H.S. 2004, American Scientific Pub., vol. 8, pp 593−615.

(38) MacMahon, S.; Fong II, R.; Baran, P. S.; Safonov, I.; Wilson, S. R.; Schuster, D. I. Synthetic approaches to a variety of covalently linked porphyrin-fullerene hybrids. *J. Org. Chem*. **2001**, *66*, 5449–5455.

(39) Li, K.; Schuster, D. I.; Guldi, D. M.; Herranz, M. A.; Echegoyen, L. Convergent synthesis and photophysics of [60]fullerene/porphyrin-based rotaxanes. *J. Am. Chem. Soc*. **2004**, *126*, 3388–3389.

(40) Huang, Y. Y.; Sharma, S. K.; Dai, T.; Chung, H.; Yaroslavsky, A.; Garcia-Diaz, M.; Chang, J.; Chiang, L. Y.; Hamblin, M. R. Can nanotechnology potentiate photodynamic therapy?. *Nanotechnol. Rev*. **2012**, *1*, 111–146.

(41) Sperandio, F. F.; Gupta, A.; Wang, M.; Chandran, R.; Sadasivam, M.; Huang, Y.-Y.; Chiang, L. Y.; Hamblin, M. R. Photodynamic therapy mediated by fullerenes and their derivatives. *Biomed. Nanomed. Technol. (B&NT)*: Concise Monographs Series **2013**, 1–51. ISBN: 9780791860083, ASME Press, New York.

(42) Elim, H. I.; Jeon, S.-H.; Verma, S.; Ji, W.; Tan, L.-S.; Urbas, A.; Chiang, L. Y. Nonlinear optical transmission properties of C_{60} dyads consisting of a light-harvesting diphenylaminofluorene antenna. *J. Phys. Chem. B* **2008**, *112*, 9561−9564.

(43) Saito, S.; Oshiyama, A. Cohesive Mechanism and Energy Bands of Solid C_{60}. *Phys. Rev. Lett.* **1991**, *66*, 2637–2640.